AIDA

Advanced European Infrastructures for Detectors at Accelerators

Milestone Report

Design of TASD and MIND

Noah, Etam (University of Geneva) *et al*

26 November 2012

This work is part of AIDA Work Package **8: Improvement and equipment of irradiation and test beam lines**.

Grant Agreement No: 262025

AIDA

Advanced European Infrastructures for Detectors at Accelerators

Seventh Framework Programme, Capacities Specific Programme, Research Infrastructures, Combination of Collaborative Project and Coordination and Support Action

MILESTONE REPORT

DESIGN OF TASD AND MIND

MILESTONE: MS28

Document identifier:	AIDA-MS28-v1.0.docx
Due date of milestone:	End of Month 20 (September 2012)
Report release date:	26/11/2012
Work package:	WP8: Improvement and equipment of irradiation and beam lines
Lead beneficiary:	Geneva University
Document status:	Final (pending approval by steering committee!)

Abstract:

Within the AIDA project, feasibility studies of plastic scintillator-based TASD and MIND detectors with SiPM readout for future accelerator-based neutrino physics are carried out under task WP8.5.2. The aim is to simulate, develop and characterise such detectors at the H8 beam line in the North Area at CERN. This milestone report outlines the design of the TASD and MIND prototypes.

Delivery Slip

	Name	**Partner**	**Date**
Authored by	E. Noah	UNIGE,	02/11/12
Edited by	E. Noah, A. Blondel, P. Soler	UNIGE, CERN, UNIGLA	26/11/12
Reviewed by	M. Moll [WP coordinator] L. Serin [Scientific coordinator]	CERN CNRS	
Approved by	Steering Committee	-	

1. PARAMETER LIST

1.1. TASD PARAMETERS

Table 1:   TASD prototype parameters.

Parameter	Symbol	Unit	Nominal Value	Range Min	Range Max
Detector global dimensions					
Detector width	w_{det}	m	1.0	0.9	1.1
Detector height	h_{det}	m	1.0	0.9	1.1
Detector depth	d_{det}	m	0.75	-	-
Detector depth with gaps	d_{gap}	m	197.5	-	-
Plastic scintillator					
Material	-	-	Polystyrene		
Number of planes per module (xy or uv)	-	-	2	1	2
Number of modules	n_{module}	-	50		
Gap between planes within module		cm	0	0	0.05
Module envelope thickness	t_{env}	cm	0.05	0	0.05
Scintillator bar length	l_{sci}	cm	90.0	80.0	100.0
Scintillator bar width	w_{sci}	cm	1.0	1.0	3.0
Scintillator bar height	h_{sci}	cm	0.7	0.6	1.0
Bars per plane	n_{bars_pla}	-	90		
Bars per module	n_{bars_mod}	-	180		
Total number of bars	n_{bars_tot}	-	9000		
Gap between scintillator modules					
Number of gaps	n_{gaps}		49		
Gap thickness	t_{gap}	cm	2.5	0.0	2.5
Material	-	-	air		
Light readout and conversion					
Light readout optical fibres		-	WLS	C.F.	
Total length of fibre	l_{fibre}	m	12000	10000	20000
Readout device	-	-	SiPM		
Readout from One/Two sides	-	-	1		

1.2. MIND PARAMETERS

Table 2:   MIND prototype parameters.

Parameter	Symbol	Unit	Nominal Val.	Range Min	Range Max
Detector global dimensions					
Detector width	w_{det}	m	3.0	2.5	4.0
Detector height	h_{det}	m	1.5	1.0	2.0
Detector depth	d_{det}	m	2.3	2.0	3.0
Iron plates					
Number of plates	n_{iron}	-	51		
Iron width	W_{iron}	m	3.0	2.5	4.0
Iron height	H_{iron}	m	1.5	1.0	2.0
Iron thickness	T_{iron}	cm	3.0	2.0	5.0
Total iron weight	m_{iron}	tons	54		
Total iron area	A_{iron}	m^2	230		
Number of slots for coil	n_{slots}	-	2	2	4
Slot for coil: width	w_{slot}	cm	10.0		
Slot for coil: height	h_{slot}	cm	20.0		
Support structure		-	TBD		
Gap between steel plates					
Number of gaps	n_{gaps}		50		
Gap thickness	t_{gap}	cm	1.5	1.2	2.0
Material	-	-	air + plastic		
Plastic scintillator					
Material	-	-	Polystyrene		
Number of planes per module (xy or uv)	-	-	2	1	2
Number of modules	n_{module}	-	50		
Gap between planes within module		cm	0	0	0.05
Module envelope thickness	t_{env}	cm	0.05	0	0.05
Scintillator bar length	l_{sci}	cm	90.0	80.0	100.0
Scintillator bar width	w_{sci}	cm	1.0	1.0	3.0
Scintillator bar height	h_{sci}	cm	0.7	0.6	1.0
Bars per plane	n_{bars_pla}	-	90		
Bars per module	n_{bars_mod}	-	180		
Total number of bars	n_{bars_tot}	-	9000		
Light readout and conversion					
Light readout optical fibres		-	WLS	C.F.	
Total length of fibre	l_{fibre}	m	12000	10000	20000
Readout device	-	-	SiPM		
Readout from One/Two sides	-	-	1		

2.   INTRODUCTION

AIDA (Advanced European Infrastructures for Detectors at Accelerators) is a 4-yr project partly funded by the EU under the FP7 Research Infrastructures programme, which started in February 2011. It aims to upgrade, improve and integrate key European research infrastructures and develop advanced detector technologies for future particle accelerators.

Within the AIDA project description, task WP8.5.2 has been set-up to study specific issues related to plastic scintillator detectors for future accelerator-based neutrino facilities.

This document describes the motivation for such developments, a timeline and "relative" costing for task WP8.5.2.

2.1.   MOTIVATION

The last decade has brought major results in the field of neutrino physics, each one helping to redefine the direction of operational and future neutrino experiments. Typical of this process are the latest measurements, those showing a large $sin^2 2\theta_{13}$, by the Daya Bay [1] (March 2012: $sin^2 2\theta_{13} = 0.092 \pm 0.016 (\text{stat}) \pm 0.005 (\text{sys})$) and Reno [2] (April 2012: $sin^2 2\theta_{13} = 0.113 \pm 0.013 (\text{stat}) \pm 0.019 (\text{sys})$)) collaborations.

For the next decade, (soon to be) operational facilities such as accelerator-based experiments NOνA, T2K, MINOS, ICARUS and OPERA and reactor-based experiments Double Chooz, Daya Bay and Reno are expected to provide increasing precision on measured parameters such as θ_{13}, θ_{23}, $|\Delta m^2_{31}|$.

For the next generation neutrino facilities a re-assessment is underway as to how to study the established remaining unknowns such as the CP-violation phase, δCP, mass hierarchy and the postulated existence of sterile neutrinos. Some indications are emerging, suggesting substantial changes to key parameters for planned facilities, and several very recently published proposals for new accelerator-based facilities briefly described in the following:

- Long baseline neutrino oscillation experiment (LBNO) [3], Expression of Interest, June 2012.
- "Short" baseline neutrino experiment [4], Technical proposal, March 2012.
- The long baseline neutrino experiment (LBNE) [5] in the USA, Conceptual Design Report, October 2012.
- The Hyper-Kamiokande Experiment [6] in Japan, Letter of Intent, September 2011.
- A prototype muon storage ring proposal, νSTORM [7] in the USA, Letter of Intent, June 2012.
- International Design Study for the Neutrino Factory (IDS-NF) [8]: μ momentum revised from 25 GeV/c to 10 GeV/c.

The LBNO EoI dated 28th June 2012 outlines a proposal for a new neutrino beamline facility (CN2PY). Neutrinos produced with the CERN SPS accelerator would be sent to a new far detector complex located at a distance of 2300 km in the deepest mine in Europe at Pyhäsalmi (Finland). A double phase 20 kton liquid argon (LAr) Large Electron Multiplier Time Projection Chamber (LAr LEM-TPC) will provide the required tracking and calorimetry performance whilst downstream of the LAr detector a magnetized iron calorimeter with muon momentum and charge identification will collect an independent neutrino sample and act as a tail catcher for events occurring in the LAr. These detectors serve the physics objectives of investigating all flavour oscillations (ν_μ to ν_μ, ν_μ to ν_τ, ν_μ to ν_e) with neutrinos and

antineutrinos, explicitly testing the existence of CP-violation and conclusively determining mass hierarchy for any value of δ_{CP}.

The technical proposal for a short baseline neutrino experiment dated 15th March 2012 outlines the case for a new CERN-SPS neutrino beam to search for sterile neutrinos beyond the Standard Model. The ICARUS T600 LAr TPC is the core detector, along with another smaller LAr TPC (T150) located respectively 1600 m and 300 m from the proton target. Downstream of each LAr TPC, a magnetised iron detector will perform muon momentum and charge identification from low energy (< 1 GeV) over a wide energy range and transverse area > 50 m^2, allowing the separation of ν_μ from anti-ν_μ and therefore controlling systematics from muon mis-identification at high momenta.

LBNE is a proposal in the USA currently being reconfigured to better manage costing. The latest steering committee report dated 6th August 2012 outlines three possibilities with different baselines and detector sizes, of which the favoured option is to place in a first phase a 10 kton liquid argon time projection chamber at Homestake on the surface, 1300 km from a new beamline at Fermilab.

The Hyper-Kamiokande detector is proposed as a next generation underground water Cherenkov detector based on the well proven technology of T2K, with a fiducial volume a factor 25 larger. It would serve as a detector for a new long baseline neutrino oscillation experiment taking beam from an upgraded 1.66 MW J-PARC proton synchrotron. Its capabilities would also extend far beyond those of T2K in observing proton decays, atmospheric and cosmic neutrinos.

At νSTORM, beams of ν_e (anti-ν_e) and anti-ν_μ (ν_μ) are produced from the decay of a stored 3.8 GeV μ^+ (μ^-) beam at Fermilab. Near detectors would measure neutrino-nucleus scattering cross-sections at the percent level in the range $0.5 < E_\nu < 3$ GeV, knowledge of which is required for next generation long baseline neutrino experiments. A combination of a near (50 m) and far (~2 km) magnetised iron detectors would provide sensitive searches for active/sterile neutrino oscillations in both the appearance and disappearance channels.

Another relevant proposal is the Indian Neutrino Observatory (INO), a proposal for a large 50 ktons magnetised iron calorimeter with resistive plate chambers as the active detector elements for atmospheric neutrinos.

The recent re-evaluation of facilities carries consequences for the neutrino detectors. As can be seen from the majority of proposals listed above, plastic scintillators as trackers or tracking calorimeters with/without magnetic fields are considered to be an important part of the main detector options.

2.2. STUDYING SOLID SCINTILLATOR DETECTORS

The use of solid polystyrene-based scintillators is widespread amongst the neutrino physics community, latest relevant examples include:

- the MINOS detectors (near and far),
- the T2K near detectors (off-axis SMRD, on-axis INGRID & INGRID proton module),
- the MINERvA detector.

Along with the performance of these detectors obtained online, dedicated test runs have provided valuable information, for example the calibration detector tests or CalDet carried out for MINOS which measured the energy resolution for the setup to be 21.42%/√E (GeV), 56.6%/√E (GeV) and 56.1%/√E (GeV) for electrons, protons and pions respectively [9]. Much

of this information is useful in designing future detectors although different readout schemes going from the MINOS detector photomultiplier tubes to silicon photomultipliers, and different geometries with finer segmentation call for detailed testing.

Some of the characteristics of the above detectors are poorly known, either because they have not been tested or because the conditions under which tests were carried out were not representative of the operational environment (e.g. no B-field). There is a strong incentive to study:

- For the Totally Active Scintillating Detectors (TASD):

  ➢ Stopping properties of pions and muons. Test beam: 200 MeV/c . This will be studied with the MICE EMR detector.

  ➢ Electron and muon charge separation inside a magnetic field, in particular electron charge ID in electron neutrino interactions for the platinum channel at a neutrino factory. Test beam: 0.5 – 5 GeV/c (AIDA – Morpurgo).

- For the Magnetised Iron Neutrino Detectors (MIND):

  ➢ Muon charge identification, for wrong sign muon signature of a neutrino oscillation event: golden channel at a neutrino factory: requires correct sign background rejection of 1 in 10^4, 0.8 - 5 GeV/c.

  ➢ Hadronic shower reconstruction for identification of charged current neutrino interactions and rejection of neutral current neutrino interactions. Test beam: protons/pions 0.5 – 9 GeV/c.

The large-scale detectors planned for future facilities, and requirements for ever increasing resolution and hence finer segmentation of the plastic scintillators lead to an increase in the number of channels. It then becomes important to optimise the cost/channel for the readout scheme.

2.3. NEAR VS FAR DETECTORS

Most planned accelerator-based neutrino experiments envisage a near detector located close to the neutrino source and a far detector located some distance away, typically 1-2 km for short baseline experiments or hundreds of km for long baseline experiments. These often have significant differences:

- the flux is much higher at the near detector and is not isotropic.

- the neutrino energy spectrum is different.

- the cosmic background is usually much higher at a near detector since it is rarely installed deep underground.

- the near detector is smaller so full containment of tracks can be an issue.

Because of their size and the incident particle rates, the prototype TASD and MIND detectors are much closer in functionality to near detectors, yet results from their characterisation must also serve the design of far detectors.

3. BEAMLINE REQUIREMENTS

The beamline requirements for a low energy test beam to study the properties of future neutrino detectors are reported in the AIDA Milestone Report MS27 [10]. They are summarised here for consistency. The test beam is required to deliver electrons, muons and hadrons (pions and protons) in a momentum range between 0.5 and 5.0 GeV/c with the possibility of extending up to 9 GeV/c. A large aperture magnet such as the MORPURGO magnet installed in the North Area at CERN should be included in the test beam infrastructure. A possible location is the H8 beamline at the North Area (which includes the MORPURGO magnet) but could also be in the East Area which would require the installation of a suitable magnet. These options are studied as part of AIDA WP8.2.

A possible implementation is shown in Figure 1. The bend is required because the proton beam impinging on the secondary target will create high energy muons ~40-100 GeV, beam size 1 x 1 m^2, which would be a significant background for the detectors. If the bend is not implemented, a high resolution ~10 ps, large area (1×1 m^2) time of flight detector would be required just after the secondary target to veto the high energy muons.

Close collaboration between detector studies and beam studies is required because a number of parameters such as particle rate, beam size and angle of incidence on the detector will affect the detector design.
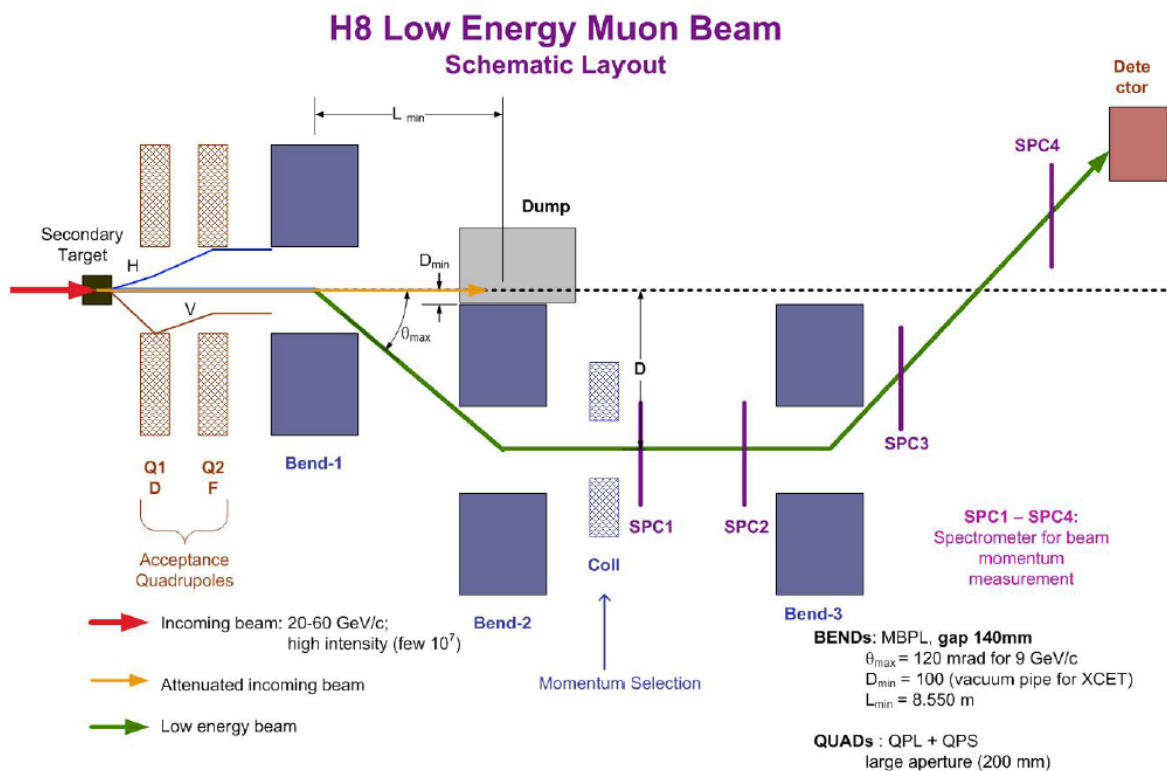

Figure 1:   Possible implementation of a low energy muon test beam. Note that since it is planned to have the MIND detector located downstream of the TASD detector (assuming the TASD is installed in the MORPURGO magnet), the particle beam must be parallel to the axes of both the TASD and the MIND.

3.1. PARTICLE RATES

Particle rates presented in Table 3 are given as an indication, in order to have a rough idea of the estimated beam time for sufficient statistics, and for an upper limit to be considered in the design of the electronics and data acquisition chains. Significant departures from these values are expected when studies of the beamline in WP8.2 are carried out, especially for low momenta particles.

Table 3:   Requirements for particles and their momenta. The particle rate here is the rate within a spill, regardless of the spill length, slow extraction is assumed.

Type	Momentum values [GeV/c]	Particle rate [kHz]	Total particles	Time est.[hrs]
electron and muon charge separation: TASD in large aperture magnet (e.g. MORPURGO)				
e^{+-}	0.5, 0.7, 1.0, 2.0, 5.0, (9.0)	1	$10^6 \times 10$	17
μ^{+-}	0.5, 0.7, 1.0, 2.0, 5.0, (9.0)	1	$10^6 \times 10$	17
muon charge separation: MIND				
μ^{+-}	0.8, 1.0, 1.5, 2.0, 5.0, (9.0)	1	$10^6 \times 10$	17
hadronic shower reconstruction: MIND				
π^{+-}	0.5, 0.7, 1.0, 2.0, 5.0, 9.0	1	$10^6 \times 12$	20
p	0.5, 0.7, 1.0, 2.0, 5.0, 9.0	1	$10^6 \times 6$	10

3.2. BEAM COMPOSITION

The beam composition will be determined from simulations of the beamline carried out in FLUKA under WP8.2. An example is given here of the beam composition from the PS T7 during the MINOS CalDet tests, Figure 2 [9]. Similar data are required to know the beam contamination for each of the required particle types in Table 3. Knowledge of the momentum spread for the beam that will be received is required in order to determine whether pion/muon separation at low momenta can be done in the TASD by range.
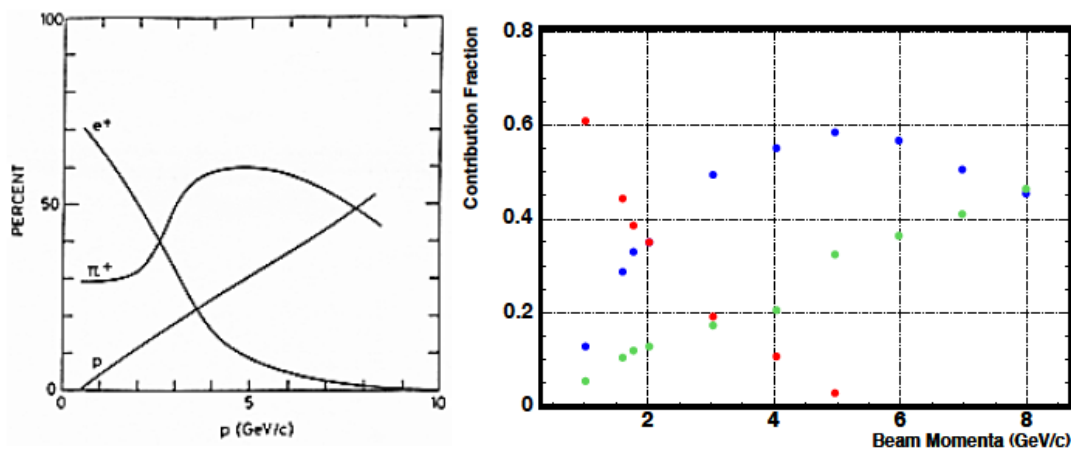

Figure 2:   PS T7 beamline particle composition. The expected composition is shown on the left. The measured composition is shown on the right [9].

3.3. MORPURGO MAGNET

The MORPURGO magnet is a good approximation to a dipole as can be seen in Figure 3, showing the XY plane. Some optimisation of the TASD detector positioning along the z-axis will be required since the peak field value drops sharply from the center of the magnet to its edges.
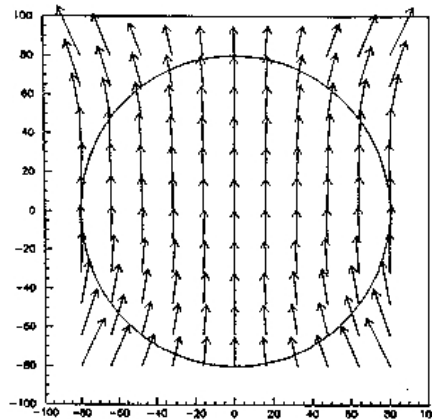

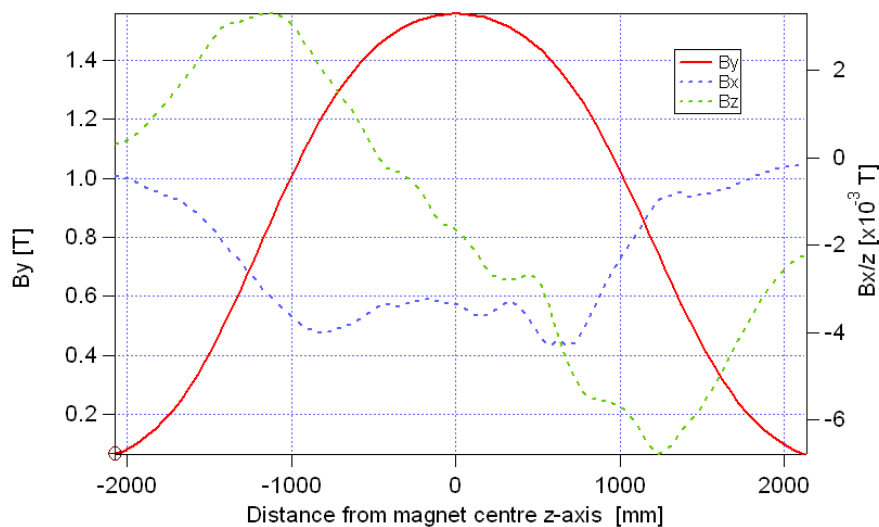*Figure 3:* *X-Y slice of the Morpurgo magnet showing the good approximation to a dipole field.*

Figure 4: *Field dependence as a function of Z for the Morpurgo magnet. As can be seen, the Z-dependence is strong. Around the centre of the magnet, for 1000 mm, the variation in the peak field value is ~10%.*

4. GENERAL DETECTOR LAYOUT

Both TASD and baby-MIND prototypes are designed with the assumption that they will be installed on the H8 beam line, in zone 158 at the North Area. They will be operated separately, which will allow for the re-use of the scintillator modules, hence cost savings. It is planned to install the TASD prototype inside the Morpurgo magnet, and the baby-MIND downstream of the TASD in one of two positions as shown in Figures 5 and 6.
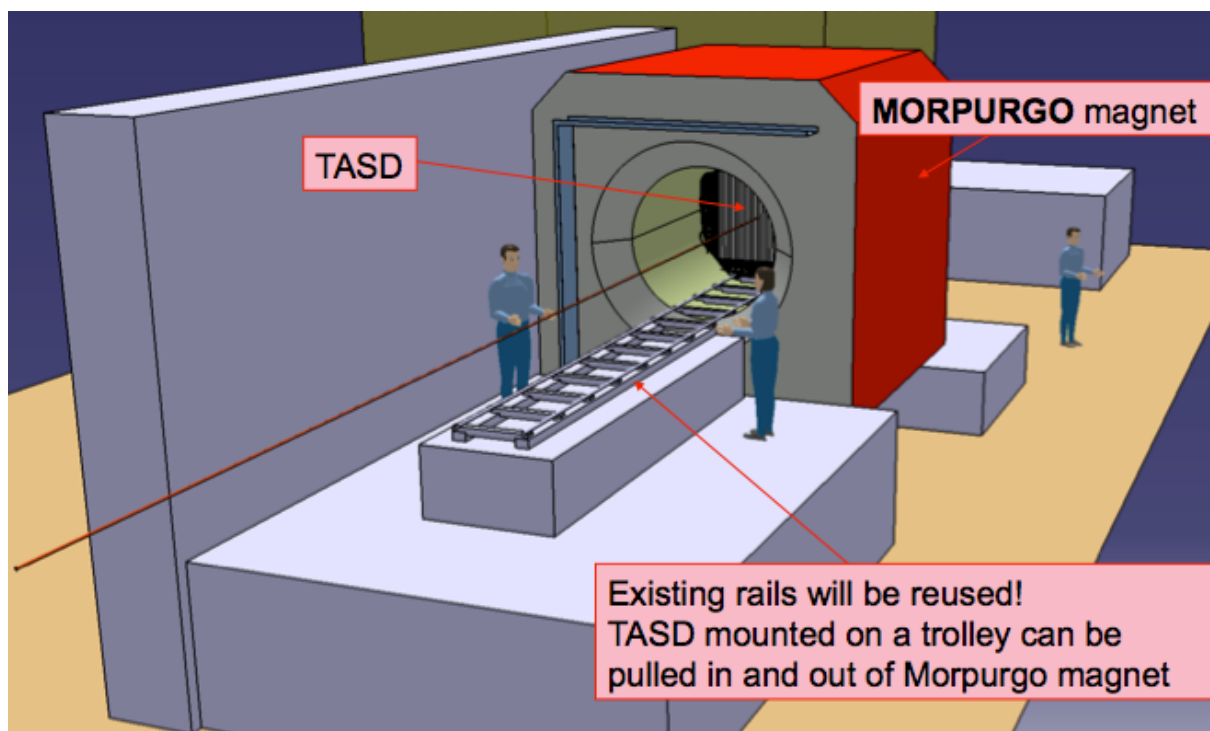

Figure 5:   Installation of the TASD inside the Morpurgo magnet volume in H8.
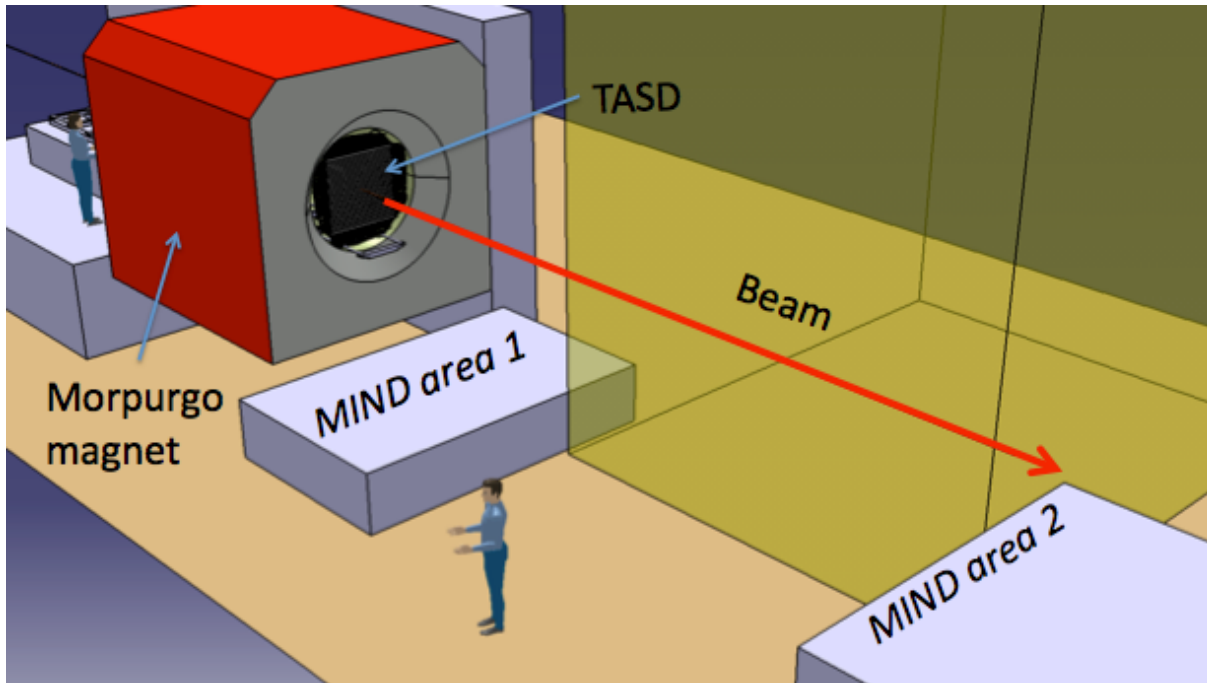
Figure 6:   Two options to position the baby-MIND detector: MIND area 1 could be used for initial tests, although the close proximity to the Morpurgo magnet is an issue to be investigated; MIND area 2 is the proposed final position of the detector.

5. TASD DESCRIPTION

5.1.   TASD DETECTOR DESIGN

The TASD detector consists of 50 modules of plastic scintillators. Each module is instrumented with one X and one Y plane, with 90 scintillator bars per plane. The plane thickness is 0.7 cm. The distance between modules can be varied from 0 to 2.5 cm. Other components either active detectors or passive sheets of material can be inserted in these 2.5 cm gaps if required. The full detector depth can therefore be varied from 75 cm to ~200 cm.

Separation by range of pions and muons of same momenta is possible at low momenta. The range in plastic of 280 MeV/c pions and muons is ~60 cm and ~72 cm respectively.

5.2.   MC STUDIES

Within the AIDA WP8.5.2, the goal is to have a software framework with a set of simulation tools that can:

- describe all the physics from beam parameters to interactions within the detector
- accurately reproduce the performance of the detectors: especially optical photon transport.
- enable an extrapolation from test beam conditions to real detector scenarios.

Table 4:   *Simulation tools for the TASD and MIND prototypes.*

Stage	Input	Output	Comment	Facility scenario		Test beam scenario	
				Near detector	Far detector	TASD	MIND
Flux driver	Machine (NF) parameters	Neutrino flux	-	custom	custom	H8 beamline simulation software	
Event generator	Neutrino flux	Vertex and outgoing particles	-	GENIE	GENIE		
Transport	vtx, particles	Energy deposits	-	GEANT4	GEANT4	GEANT4/Fluka	GEANT4/Fluka
Digitisation	Energy deposits	Electronics output	Need hardware efficiencies.	custom	custom	Geant4 (photons) custom	Geant4 (photons) custom
Energy reconstruc.	Electronics output	Est. energy deposits	-	custom	custom	custom	custom
Track reconstruc.	Electronics output, Energy deposits	Track	Rel. importance of Edep	custom	custom	custom	custom

Preliminary work has been carried out to exercise some of the tools listed in Table 4 concerning simulations of the TASD, using a basic version of the event generator, Geant4 for particle transport, and basic digitisation. Track reconstruction is work in progress, planned for a later stage in the project.

Elements of the detector geometry are parameters directly implemented in Geant4. The digitisation works by summing the energy deposited in each bar, with a poisson distribution around a mean of 15 photo-electrons/(1.8 MeV). It is planned to include light correction attenuation, and a more detailed description of SiPM response in the digitisation.

Hit maps in the XZ and XY planes of 5 GeV electrons, muons and protons are shown in figures 7, 8 and 9. The TASD detector here is in a configuration with a 2.5 cm gap between the plastic scintillator modules. The work required for track reconstruction can be appreciated. Tracking of the primary electron and secondaries produced via interactions in the TASD will require additional work. Simulations at lower momenta are also foreseen, down to 0.5 GeV/c, especially relevant for electron and muon charge identification.
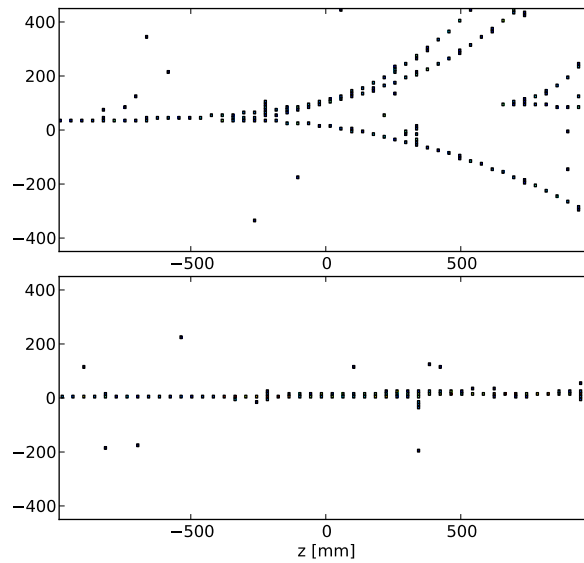
Figure 7:   Simulation of the TASD with electrons, 5 GeV. XZ and YZ planes are shown. The horizontal axis is along the Morpurgo magnet inner cylinder axis.

Figure 8:   Simulation of the TASD with protons, 5 GeV. XZ and YZ planes are shown. The horizontal axis is along the Morpurgo magnet inner cylinder axis.

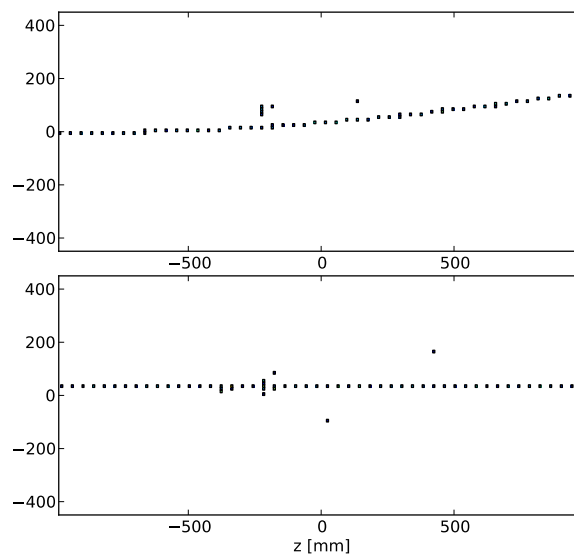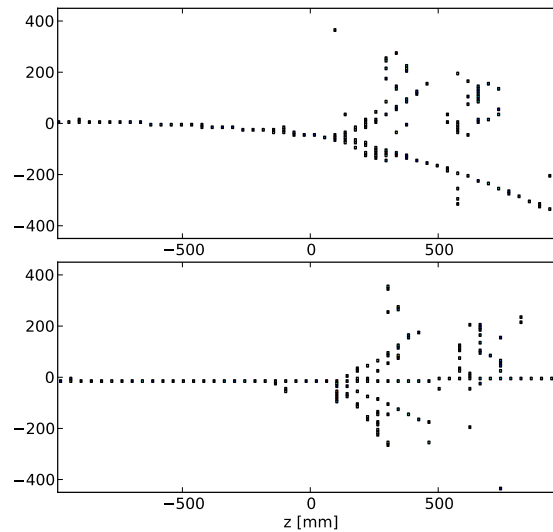*Figure 9:   Simulation of the TASD with protons, 5 GeV. XZ and YZ planes are shown. The horizontal axis is along the Morpurgo magnet inner cylinder axis.*
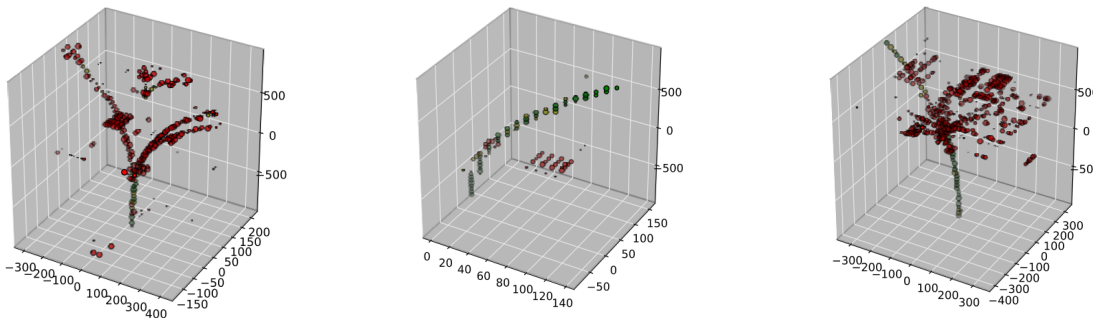

Figure 10:   3D hit maps in the TASD with basic digitisation described previously from left to right for 5 GeV electrons a), muons b) and protons c).

5.3.   TASD R&D OFFLINE

Much of the offline R&D will be carried out on the components of the TASD such as electronics, SiPMs, plastic scintillators. Since these components are shared with the MIND, they are described in a joint section further in this document.

Offline tests such as cosmic runs are foreseen on:

- subsets of the full detector, e.g. 1 plane...

- the full detector.

5.4.   TASD R&D ONLINE

The R&D online will address the full characterisation of the detector, assessing its energy and spatial resolution. Comparisons will be drawn with prior simulation work. One of the more significant elements to be checked in the simulations will be the digitisation, which requires hardware efficiencies that are measured online.

6. BABY-MIND DESCRIPTION

The Baby-MIND is a prototype for a full MIND-type detector as is planned for the LBNO detector (downstream of the LAr LEM-TPC) and *v*STORM near and far detectors. Dimensions are shown in Figures 11 and 12, to be further optimised. Assuming a minimum ionising muon looses 11.4 MeV/c per cm of steel, 51 plates of 3 cm-thick steel interleaved with 1.5 cm-thick modules of plastic scintillator would contain 2 GeV/c muons.

Due to their cost, the amount of iron is limited by mass to ~50 t, and the number of plastic scintillator modules is limited to 50. The characteristic radiation length in iron is $X_0 = 13.8$ g.cm^{-2} corresponding to 1.75 cm, or 87 radiation lengths for an iron depth of 153 cm. The characteristic nuclear interaction length in iron is $\lambda_I = 132.1$ g.cm^{-2} corresponding to 16.78 cm, or 9 interaction lengths for an iron depth of 153 cm. Although the energy resolution degrades with increasing plate thickness in the range 1-5 cm, the number of sampling points (scintillator modules) would have to be larger than the limit of 50 for this detector, especially if going for the same iron depth of 153 cm. As an example, for a 1 cm iron plate thickness, with 50 modules, the total iron depth is 51 cm and the radiation and interaction lengths scale accordingly. For larger plate thicknesses, the number of sampling points decreases (31 sampling points for 5 cm iron plates). Given the limits on iron and number of scintillator modules, a compromise for the steel thickness is 3 cm.
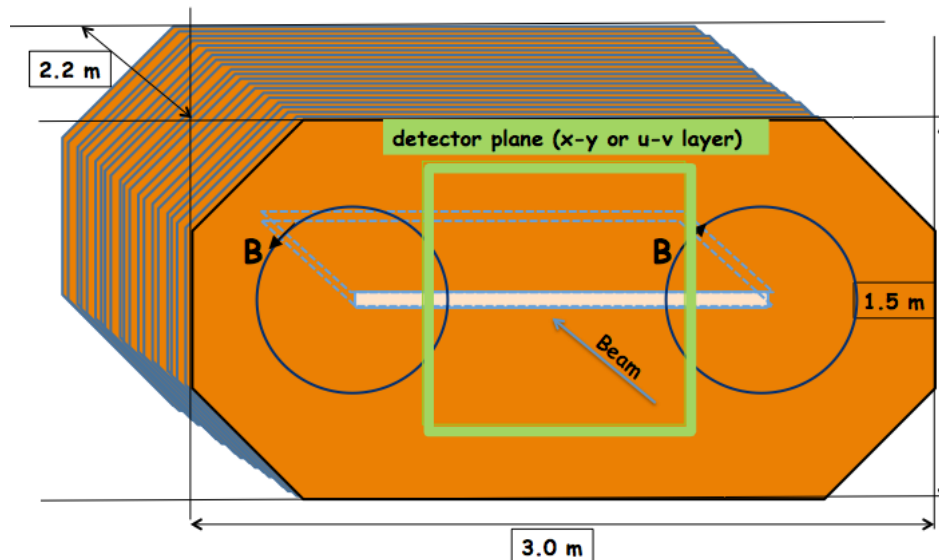

Figure 11:   Sketch illustrating the baby-MIND magnetisation principle. The baby-MIND consists of a stack of 51 steel plates, 3 cm thick, interleaved with planes of plastic scintillator detectors. The square zone delineates the volume occupied by the plastic scintillator, the circles represent magnetic field lines, the dashed line represents the conductor coil. Not shown here are the support for the steel plates and scintillator, and the slot in the steel plates for the conductor coil.
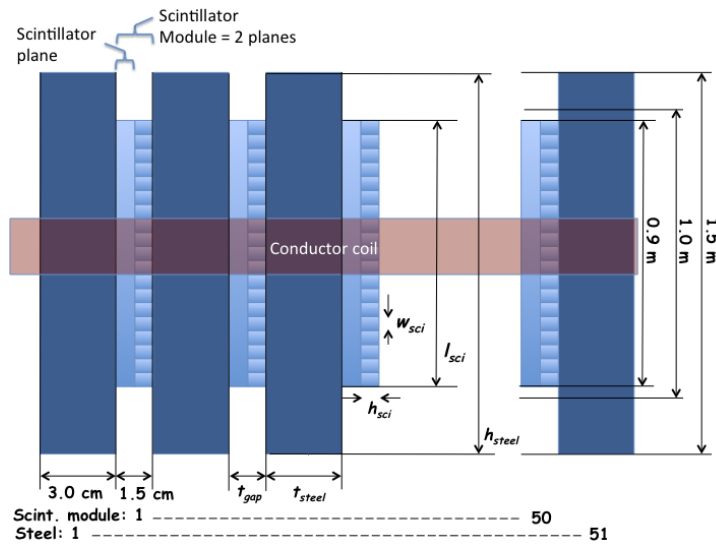
Figure 12:   Sketch of detector along beam axis, beam parallel to conductor coil.

6.1.   PERFORMANCE REQUIREMENTS

Preliminary simulations in Geant4 of a Baby-MIND are reported here. Further optimisation is ongoing, particularly concerning the geometry, definition of the magnetic field and reconstruction algorithms for pions. Assumptions taken for the geometry are octagonal plates 2 m x 1 m, two transmission lines, with a 2.8 m detector depth (along the beam axis).

Four different scenarios were tested to validate the steel thickness and for an indication of whether the choice of scintillator geometry is acceptable (0.7 cm high rectangular bars vs 1.7 cm high triangular bars), scintillator pitch = 1.0 cm in all scenarios:

- 3 cm steel plate, 1.5 cm scintillator module (i.e. 0.75 cm X plane + 0.75 cm Y plane),
- 2 cm steel plate, 1.5 cm scintillator module,
- 3 cm steel plate, 3.5 cm scintillator module,
- 2 cm steel plate, 3.5 cm scintillator module.
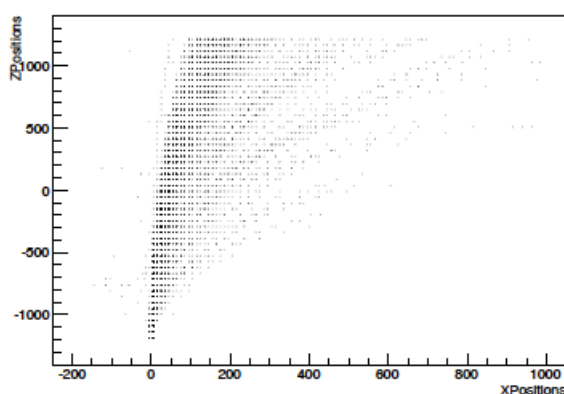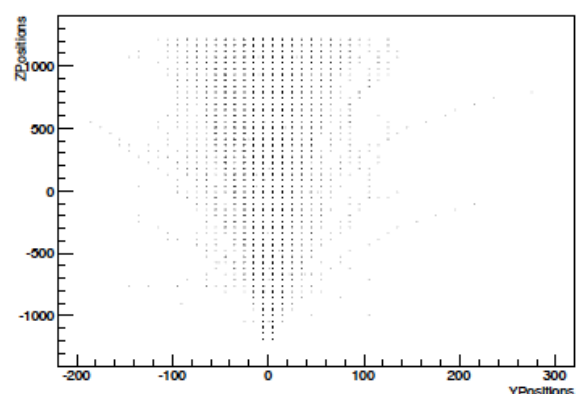
a) Z-X plane.   *b) Z-Y plane.*

Figure 13:   Tracks in reconstruction. The "active" volume follows the steel plate dimensions. Further simulations will limit the active volume to the scintillator plane

dimensions.

The Figures 13 and 14 show the muon reconstructed momenta. A uniform distribution would be expected between 0.3 GeV/c and 10 GeV/c. Further analysis is required to determine the origin of the excess around 4 GeV/c.
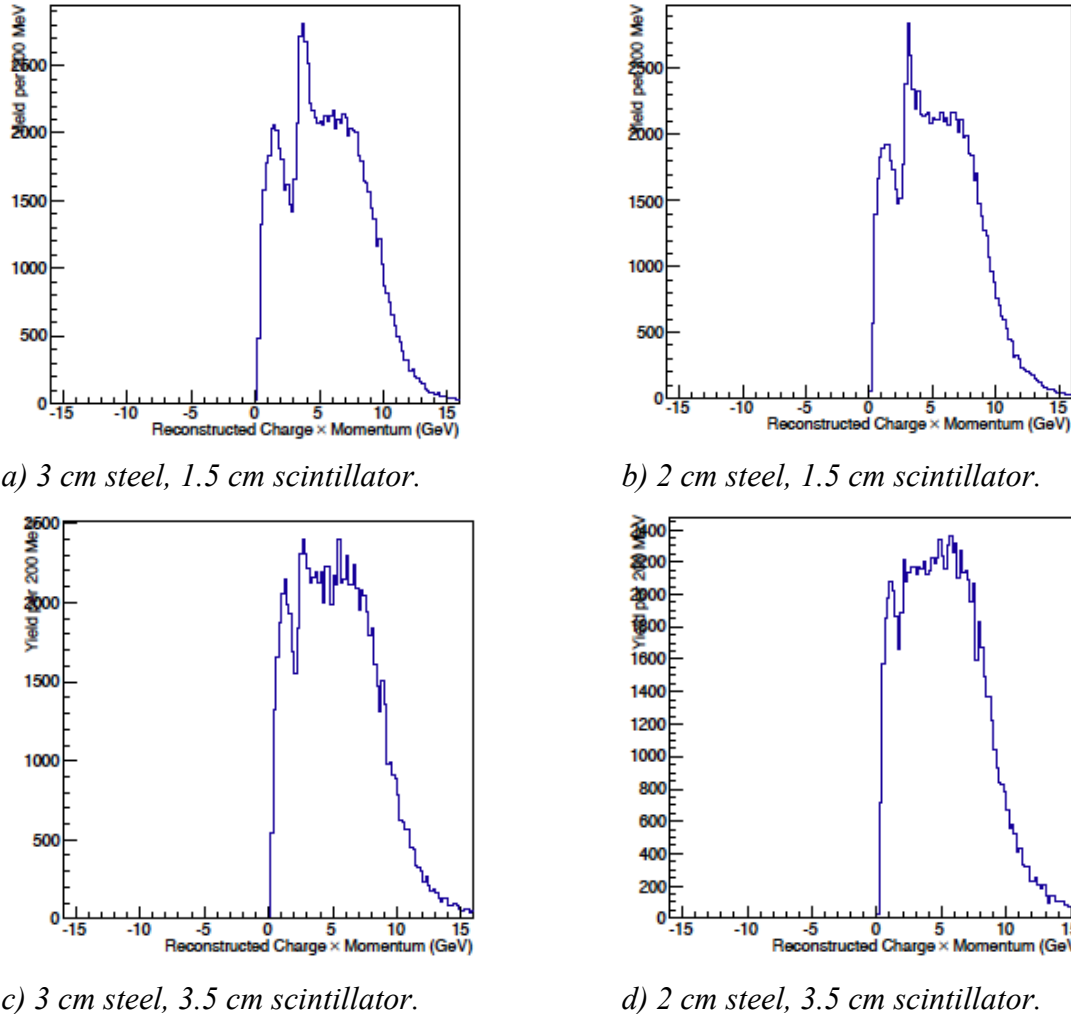

a) 3 cm steel, 1.5 cm scintillator.

b) 2 cm steel, 1.5 cm scintillator.

c) 3 cm steel, 3.5 cm scintillator.

d) 2 cm steel, 3.5 cm scintillator.

Figure 14: Reconstructed momenta for µ⁺ for different steel and scintillator combinations.

Muon reconstruction efficiencies are shown in Figure 15. All four combinations of steel and scintillator thicknesses show good efficiencies at low momenta < 2 GeV/c. The combination showing the best performance over the widest momentum range is 3.0 cm of steel and 1.5 cm of scintillator, with efficiencies close to 100% up to 6 GeV/c, staying above 99% up to 10 GeV/c. These efficiencies remain good for the other scenarios, dropping to 97% at high momenta.
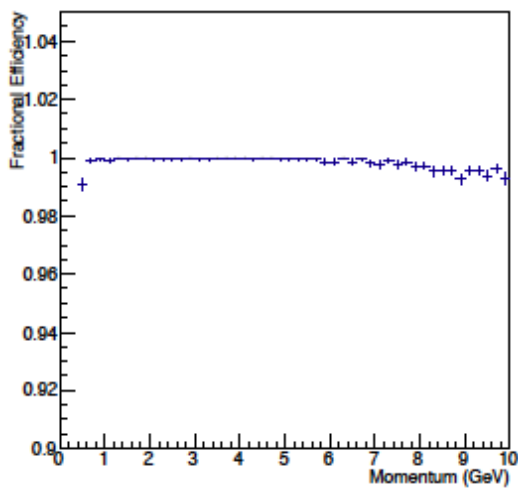
a) 3 cm steel, 1.5 cm scintillator.
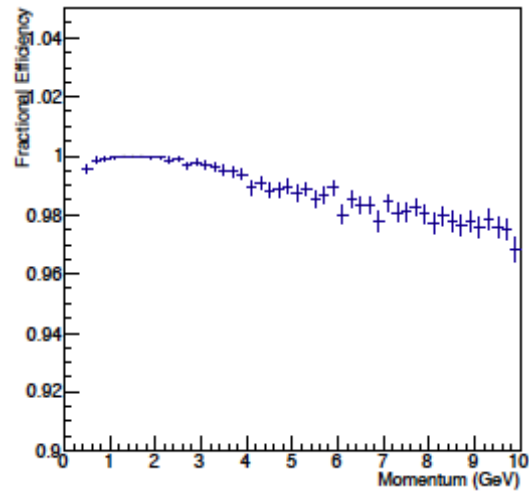
b) 2 cm steel, 1.5 cm scintillator.
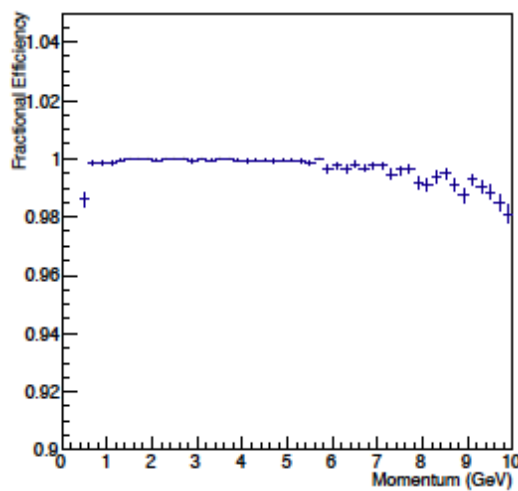
c) 3 cm steel, 3.5 cm scintillator.

d) 2 cm steel, 3.5 cm scintillator.

Figure 15:   Muon reconstruction efficiencies for different combinations of steel and scintillator thicknesses.

Charge identification efficiencies are identical for all scenarios, close to 100 % for all momenta above 1 GeV/c, Figure 16.
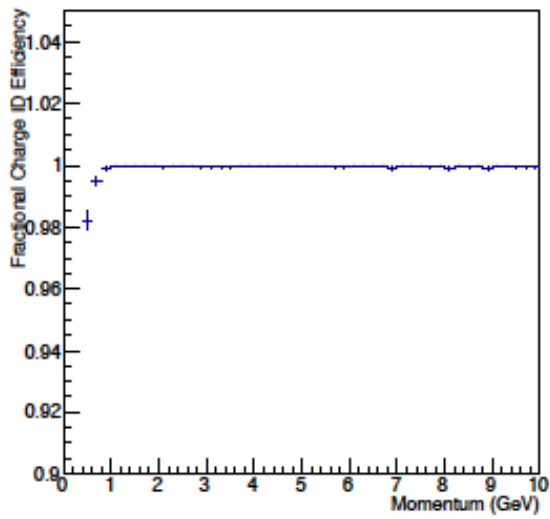
a) 3 cm steel, 1.5 cm scintillator.
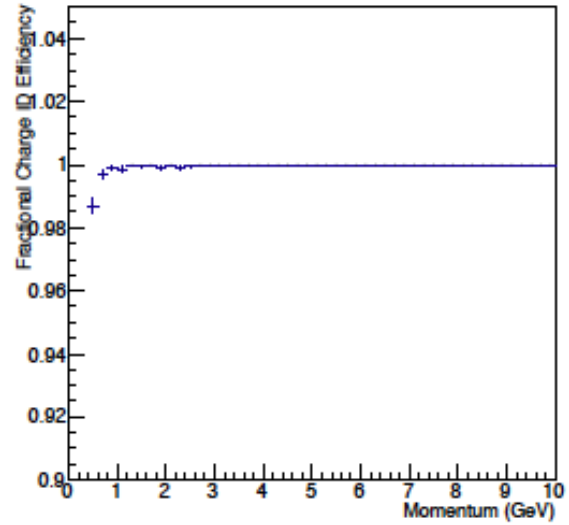
b) 2 cm steel, 1.5 cm scintillator.
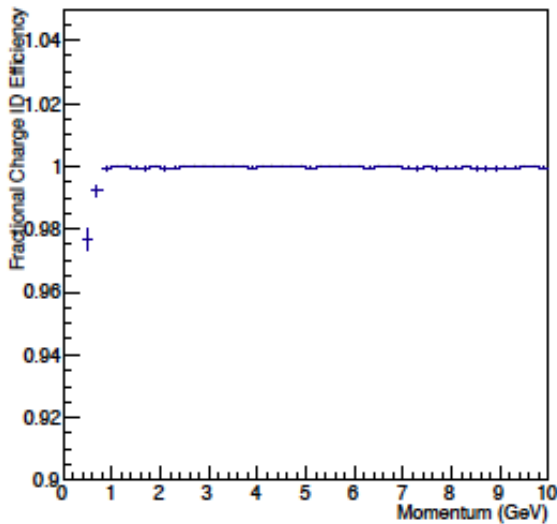
c) 3 cm steel, 3.5 cm scintillator.

d) 2 cm steel, 3.5 cm scintillator.

Figure 16:   Muon charge identification efficiencies for different combinations of steel and scintillator thicknesses.

Pion track reconstruction is more challenging because of the significant shower development, Figure 17.
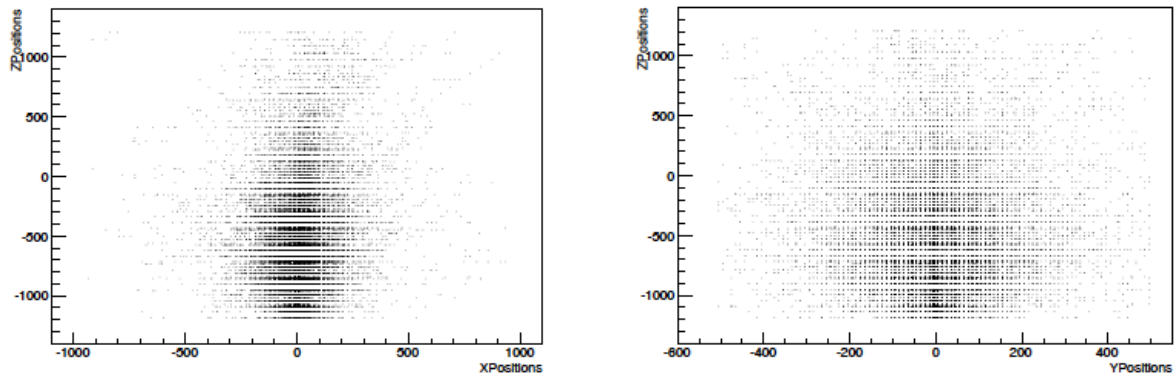
a) Z-X plane.   b) Z-Y plane.

Figure 17:   Pion showers with typical spreading. Would expect some bending to the right in Z-X view.

The pion reconstructed momenta show that individual tracks are poorly reconstructed. The input momentum distribution was uniform in p_z between 0.3 GeV/c and 10 GeV/c. The reconstructed momentum distribution is peaked at low momenta. Comparison of π^+ and π suggests some discrimination of charge although further analysis is required.
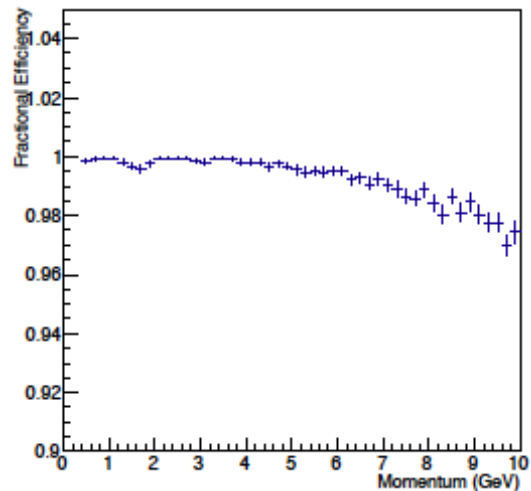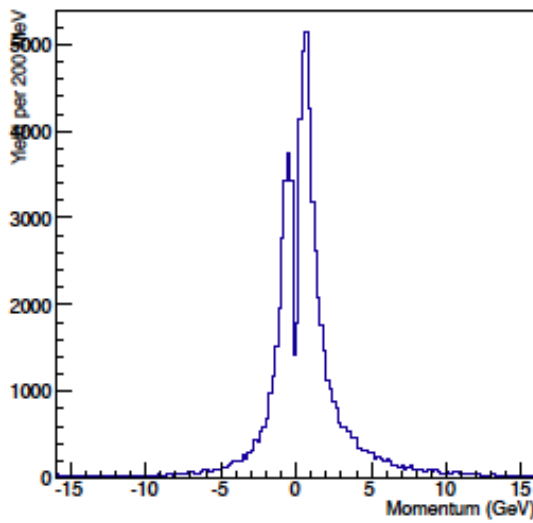
a) 3 cm steel, 1.5 cm scintillator.
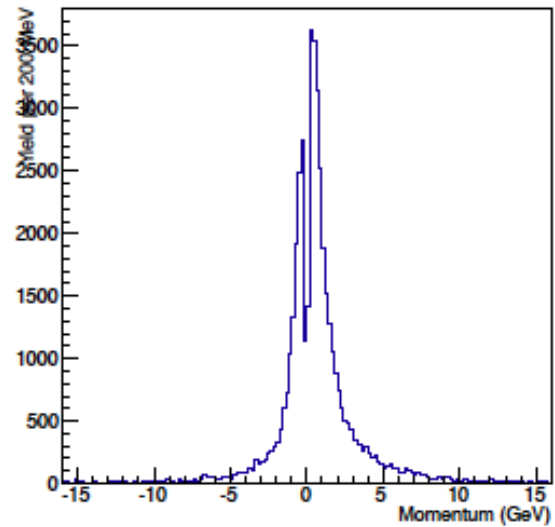
b) 2 cm steel, 1.5 cm scintillator.
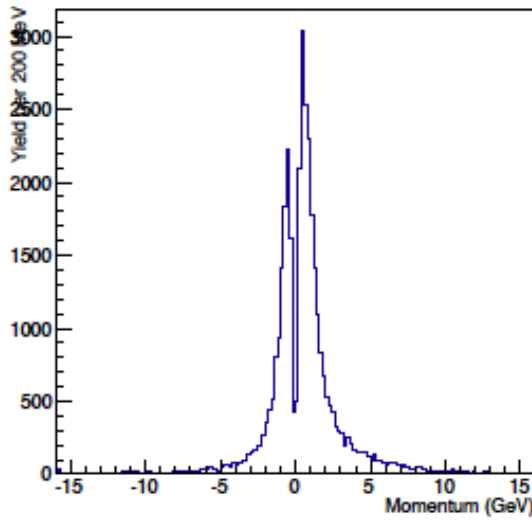
c) 3 cm steel, 3.5 cm scintillator.
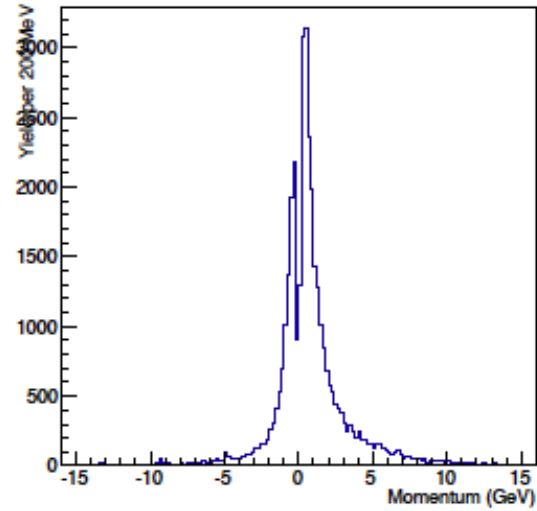
d) 2 cm steel, 3.5 cm scintillator.

Figure 18:   Reconstructed momenta for π^+.

Pion reconstruction efficiencies are shown in Figure 19.
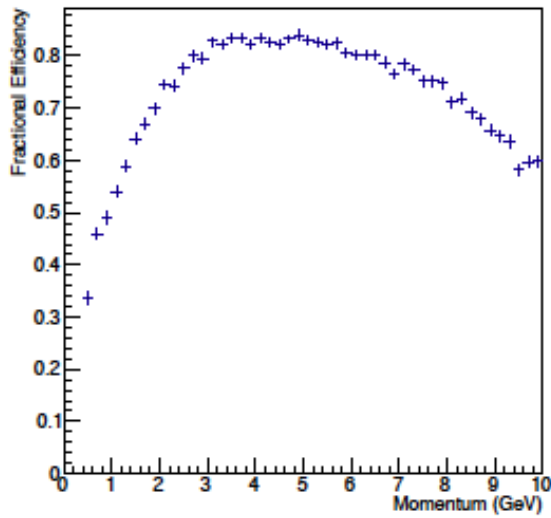
a) 3 cm steel, 1.5 cm scintillator.
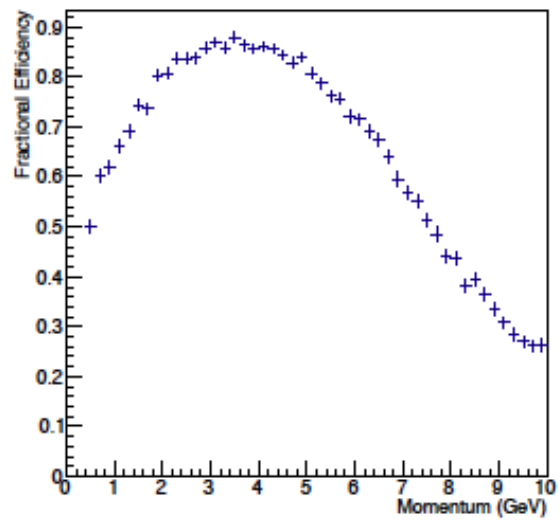
b) 2 cm steel, 1.5 cm scintillator.
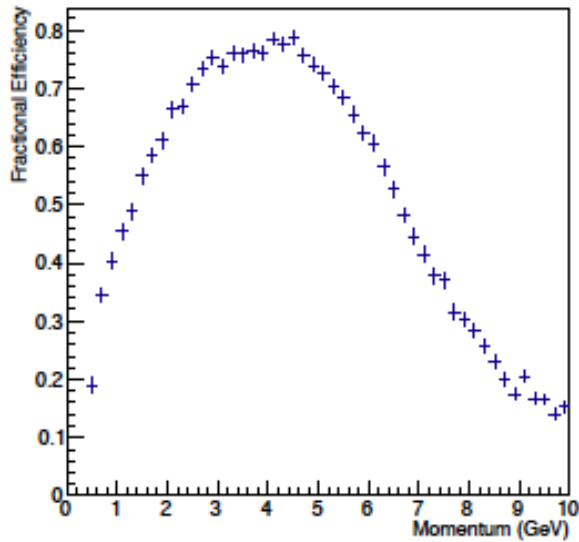
c) 3 cm steel, 3.5 cm scintillator.
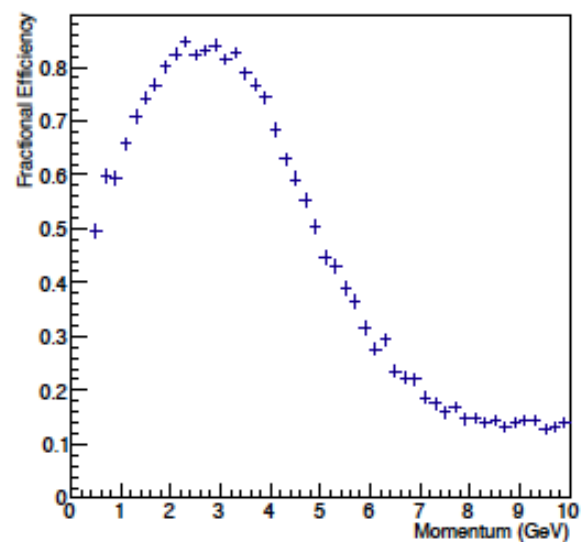
b) 2 cm steel, 1.5 cm scintillator.

Figure 19:   Reconstruction efficiencies for π^+.

Charge identification efficiencies are poor for pions, Figure 16. Single track charge identification is unreliable and requires further work.
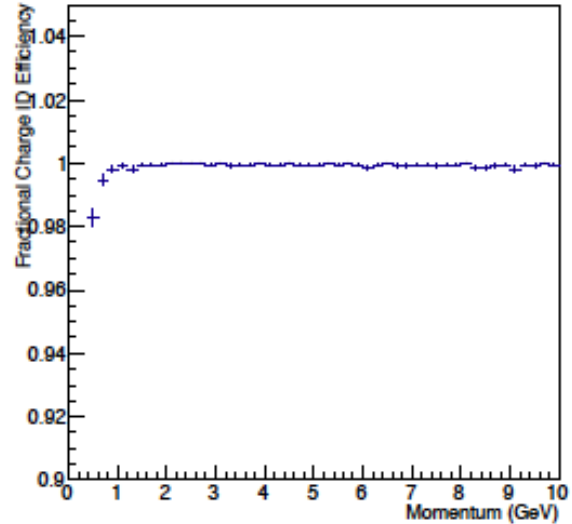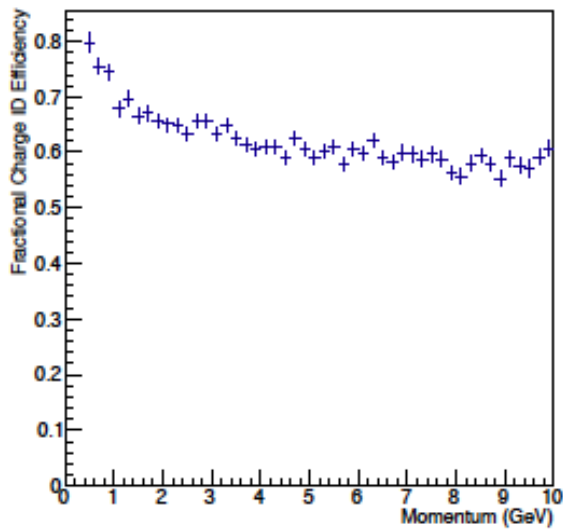
a) 3 cm steel, 1.5 cm scintillator.
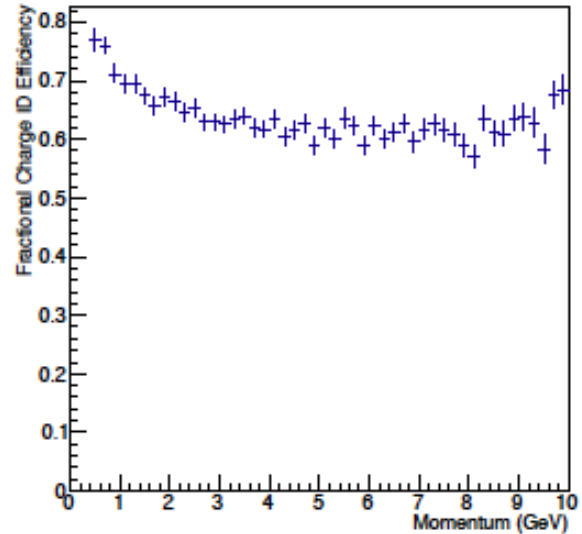
b) 2 cm steel, 1.5 cm scintillator.
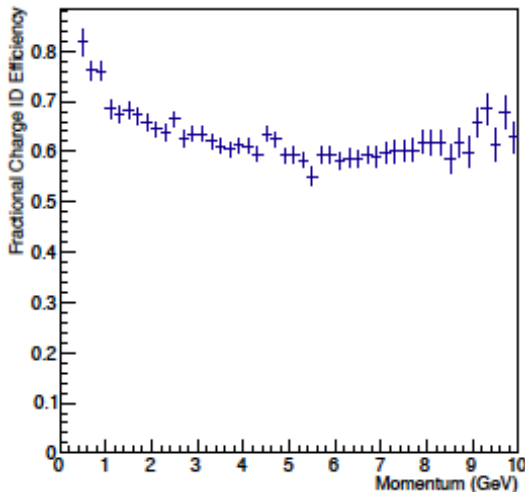
*c) 3 cm steel, 3.5 cm scintillator.*
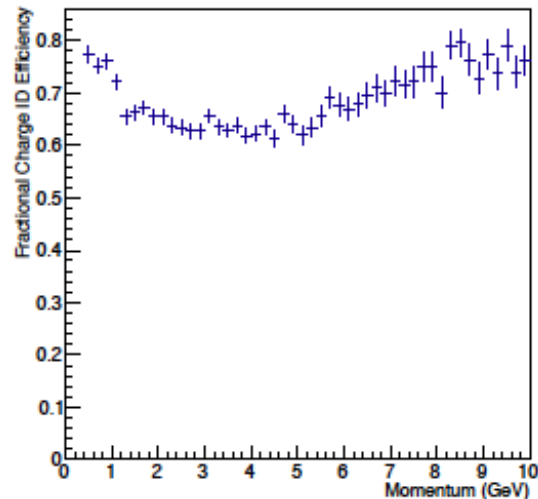
d) 2 cm steel, 3.5 cm scintillator.

Figure 20:   Charge identification efficiencies for π^+.

In summary, these preliminary simulations of track reconstruction and charge identification in the Baby-MIND indicate both for muons and pions better reconstruction efficiencies with the 3.0 cm steel plates interleaved with 1.5 cm scintillator modules.

6.2.   BABY-MIND MAGNETISATION

A low carbon steel will be selected for the baby-MIND. There are no particular radiation or environmental constraints (corrosion/humidity). The magnetisation will be set by passing a current through one or more conductor coils. Specifications for the field are the following:

- field value: 1.5 T ± 20%.
- knowledge of field in volume of interest to a precision of 1e-4, especially B_x and B_y components.
- field uniformity within steel along projection of plastic scintillator volume: 10%.
- field value outside MIND volume: maximum = 100 Gauss.

The assumption made concerning power supplies is that one can be borrowed. The coil design will therefore be made as a function of available power supplies.

Initial studies were carried out to optimise the uniformity of the B_y component of the field whilst minimising the B_x component. Although this does not represent the current consensus on MIND-type detector design, this approach was meant to minimise uncertainties in the knowledge of the B field. The resulting geometry shown in Figure 17 with two coils, led to a considerable height increase for the steel plates (factor ×2), in order to have a return path for the field lines well away from the detector plane area.
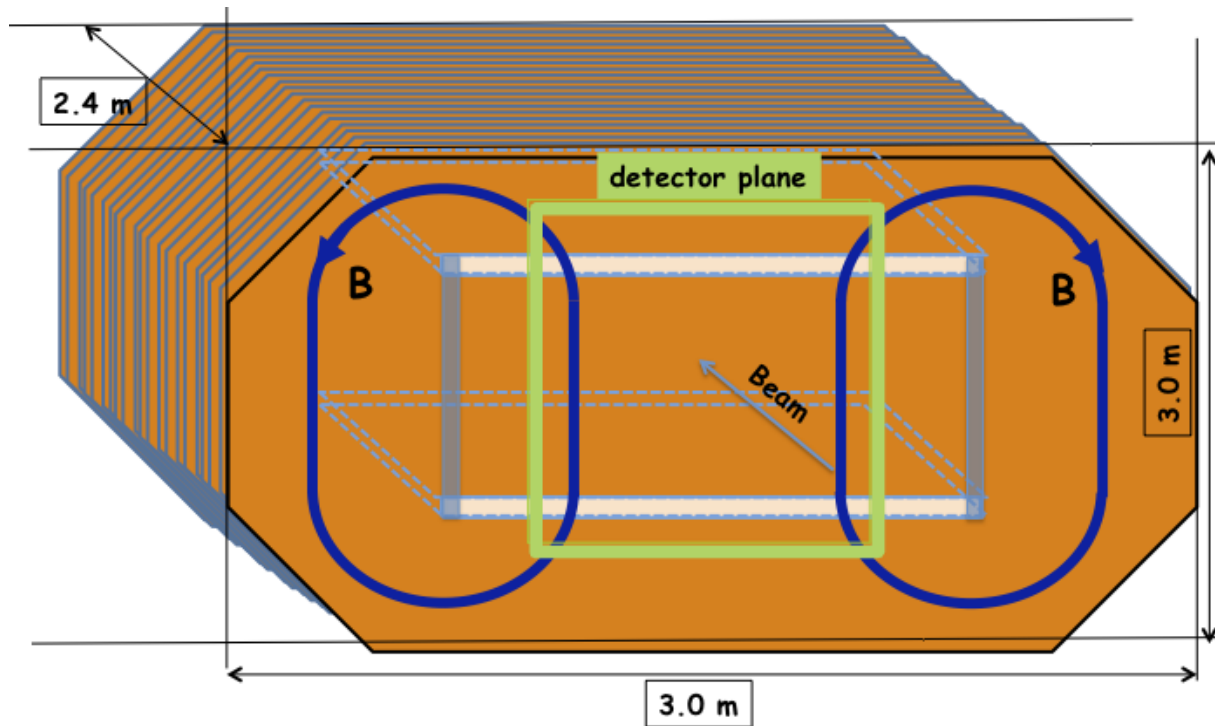
Figure 21:   Two coil solution which offers more uniform parallel B field lines in the region of interest.

Optimisation of parallel field lines imposes the following:
- two conductor coils rather than one,
- a slot between the two coils,
- double the steel height (from 150 cm to 300 cm).

Although the results of the optimisation of field lines is an impressive constraining of the B_x component of the field, 115 Gauss (0.7% of B_y) for the two coil configuration, see Figure 18, compared to 8210 Gauss (110% of B_y) for the non-optimised one coil configuration, see Figure 19, the doubling of the cost of steel and the introduction of large "empty" slots are disadvantages which drive the adoption of the one coil configuration.
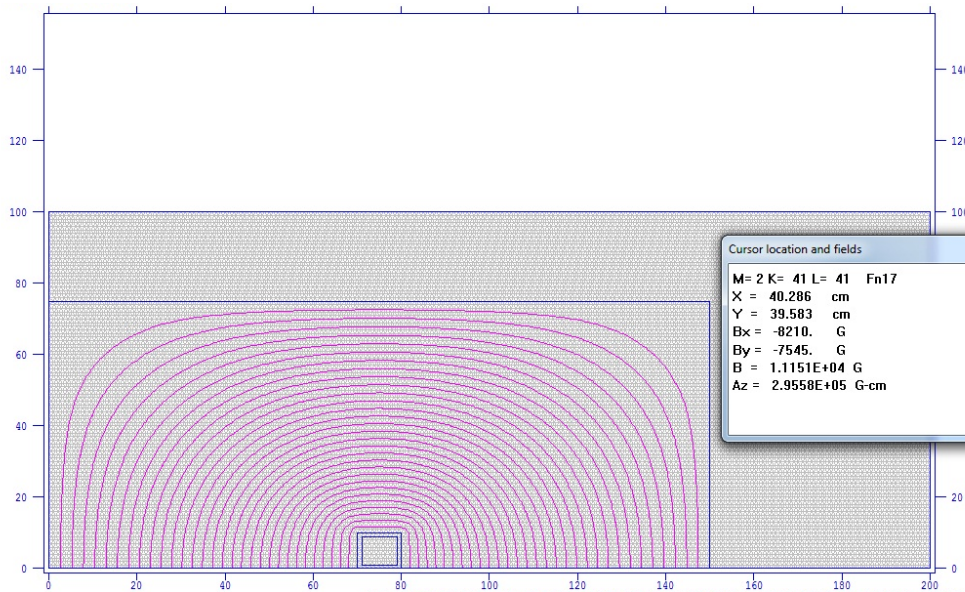
Figure 22:   Field lines calculated with a 2D code for 1/4 of the detector with a single coil represented by the small rectangle at +70 cm on the horizontal scale. The scintillator planes would extend from 0 to +45 cm on both vertical and horizontal axes (in cm). Steel extends to +75 cm on vertical axis and +150 cm on horizontal axis. Inset are values for the B_x and B_y component of the field, showing a large B_x (=110% B_y) component on the edges of the detector planes.
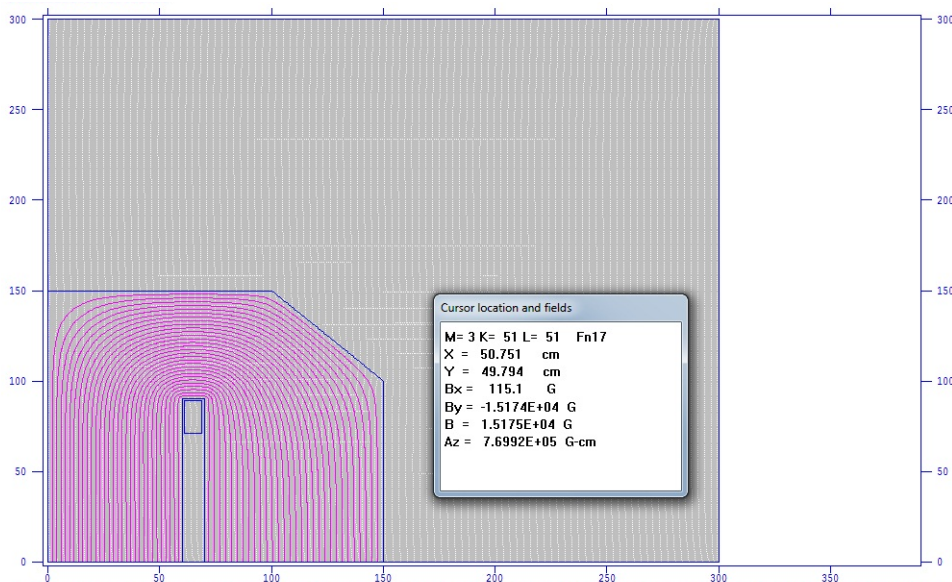
Figure 23:   Field lines calculated with a 2D code for 1/4 of the detector with two coils represented by the small rectangle at +70 cm on both scales. The scintillator planes would extend from 0 to +45 cm on both vertical and horizontal axes (in cm). Steel extends to +150 cm on vertical axis and +150 cm on horizontal axis. Inset are B_x and B_y values of the field, showing a very small B_x (=0.8% B_y) component on the edges of the detector planes.

Having chosen the one-coil configuration, attention is now turning to the challenge of determining with accuracy the value of the field, not simply the total field but separate knowledge of the B_x and B_y components of the field. One solution that has been proposed and which is currently being investigated is to create a slot away from the detector planes from the coil to the outer edge of the steel plate, into which a non-magnetised material such as a stainless steel or aluminium is inserted with an embedded magnetic field sensor. By displacing this sensor along the entire length of the gap, it is possible to create a map of the field in the gap and thus infer the field lines in the area of the detector planes.

Further optimisation work is required to produce a design for the Baby-MIND that includes detailed maps of the B field, thorough mechanical design and integration of a B field measurement system.
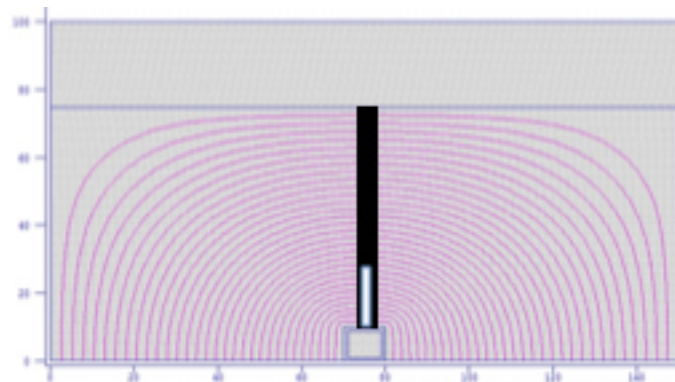
Figure 24: Sketch showing one possible method of measuring the B field by creating a gap within the steel plates and inserting a probe embedded in a non-magnetisable material. Field lines in the detector module area between 0 and +45cm on both vertical and horizontal axes can be inferred from measurements made with the probe along the gap length.
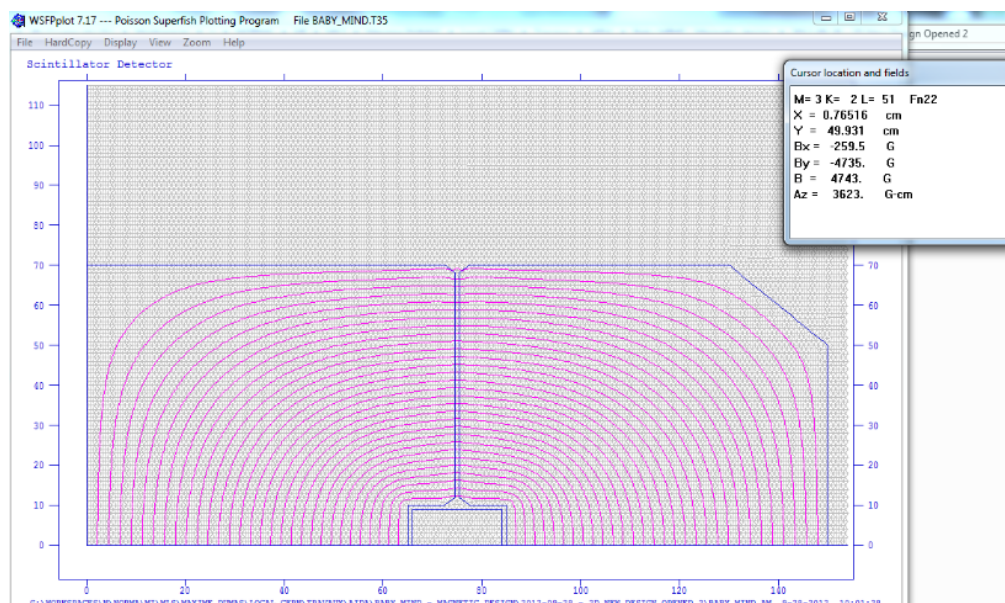
Figure 25: Simulation of the magnetic field lines for the baby-MIND with a vertical gap for the insertion of a measuring device.

6.3. R&D OFFLINE

Cosmic runs are foreseen for the baby-MIND prototype.

6.4. R&D ONLINE

The R&D online will address the full characterisation of the baby-MIND detector, assessing its energy and spatial resolution. Comparisons will be drawn with prior simulation work. One of the more significant elements to be checked in the simulations will be the digitisation, which requires hardware efficiencies that are measured online.

7. SCINTILLATOR AND FIBER READOUT

This section outlines the readout chain from the components used to the processes involved such as the initial energy deposition in the plastic scintillator, wavelength shifting and transmission of photons, SiPM conversion to photoelectrons and the conditioning of the SiPM signal by the readout electronics.

7.1. SCINTILLATORS

The scintillators will be supplied by INR. The nominal parameters for the geometry are bars of 90 cm long, 0.7 cm in height and 1.0 cm in width. A small batch of prototypes has been manufactured by Uniplast based in Vladimir (Russia) and shipped to Geneva for testing. These extruded scintillator slabs are polysterene-based with 1.5% of paraterphenyl (PTP) and 0.01% of POPOP, similar to the plastics used for the T2K SMRD detector counters. The surface is etched with a chemical agent (Uniplast) to create a 30-100 μm layer acting as a diffusive reflector. Slabs of three different sizes have been manufactured (895 x 7 x 10 mm^3, $895 \times 7 \times 20$ mm^3, $895 \times 7 \times 30$ mm^3) with 2 mm deep grooves of different widths (1.1 mm, 1.3 mm or 1.7 mm) to embed optical fibres of different diameters.
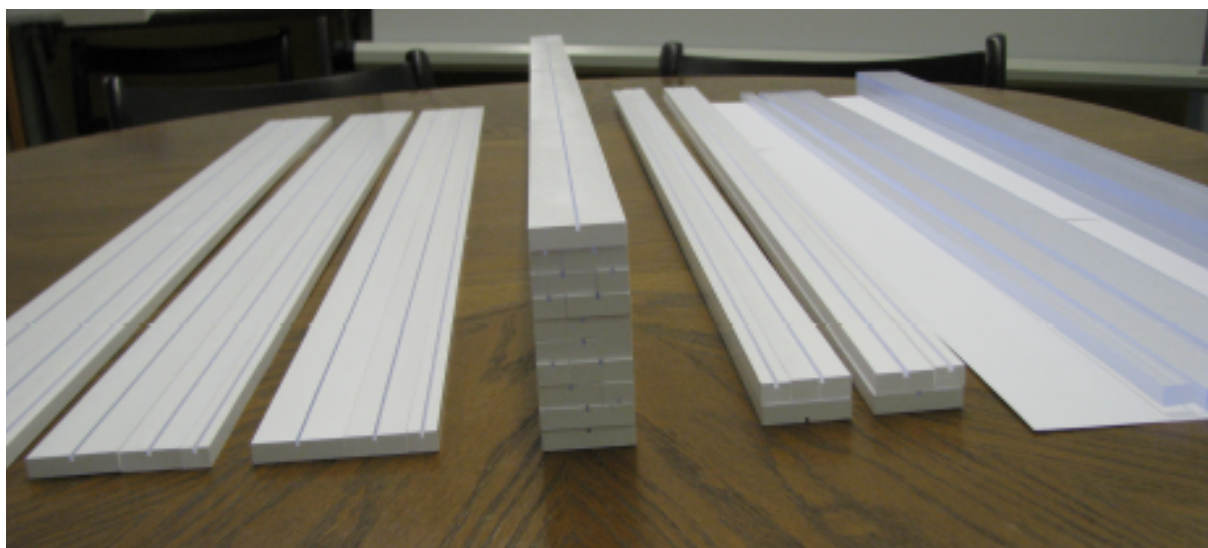
Figure 26:   Plastic scintillators produced by Uniplast.

Tests were carried out at INR to determine basic light yield and timing properties. A wavelength shifting fiber (WLS) from Kuraray (200 ppm, S-type) of d = 1.0 mm was embedded into the 1.1 mm wide groove with a silicon grease (TSF451-50M) to improve optical contact between the scintillator groove surface and the fiber. Hamamatsu MPPC photosensors (1.3 × 1.3 mm^2, 667 pixels, 50 × 50 μm^2, gain = 7.5 × 10^5 @25°C) were connected to both ends of the ~1m long WLS fibers. A cosmic telescope was set up with two trigger counters, the upper one with dimensions 7 × 7 cm^2 (for light yield checks) and 2 × 2 cm^2 (for timing checks) and the lower one with dimensions 10 × 24 cm^2. Measurements were made at the center of the scintillator slabs. The temperature during testing was 25-28°C.

Results are summarised in Table 5. They show good light yield for all bar thicknesses, the highest light yield was obtained with the narrowest 10 mm width with 83 p.e. Comparisons with/without chemical reflector show an increase of light yield of a factor 2.5 when the chemical reflector is present. The effect of the silicon grease is close to 60%. For the final assembly, the silicon grease would be replaced by glue, which is expected to have roughly the same effect. An additional Tyvek reflector provides a 20% increase in light yield, though this reflector is not currently planned for the prototype detectors.

Timing properties were studied for the two-sided readout, combining t1 and t2 with (t1-t2)/2 giving the result: $\sigma_{(t1-t2)/2}$ = 0.5 ns. The timing is mostly determined by the fiber decay constant, τ_{fiber} ~ 12 ns.

Table 5:   *Cosmic tests with prototype scintillator bars of different widths.*

Bar width [mm]	MPPC 1 [p.e.]	MPPC 2 [p.e.]	Sum [p.e.]
Bars with no chemical reflector			
10	15.7	15.8	31.5
20	15.5	13.6	29.1
30	12.8	11.5	24.3
20 + Tyvek reflector (100-120 μm)	41.8	34.8	76.6
Bars with chemical reflector			
10	46.0	36.8	82.8
20 (1) w/o grease	25.7	22.1	47.8
20 (1)	39.7	35.7	75.4
20 (1) + Tyvek reflector	49.3	44	93.3
20 (2)	32.6	28.2	60.8
30	31.2	26.6	57.8
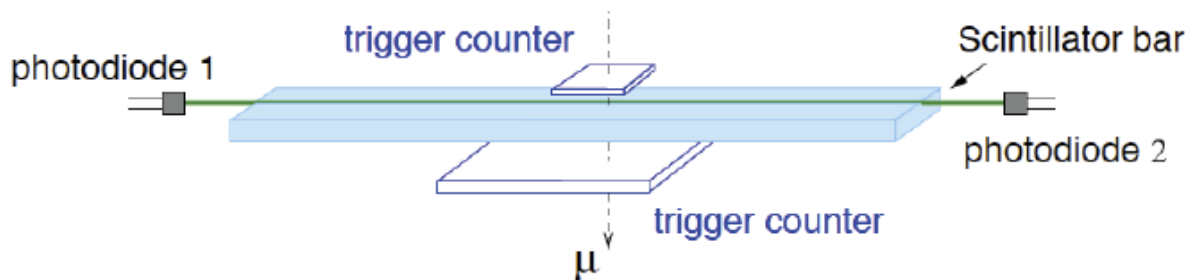
Figure 27:   Cosmic telescope set up to measure light yield and timing properties of the prototype scintillator slabs produced at Uniplast.

7.2.   SCINTILLATOR AND FIBER CONNECTORS.

A good geometrical interface between the SiPM sensitive area and the fiber is the first step in achieving good signal transmission efficiency and signal quality. Experience gained with the design of the MICE EMR optical connectors (Figure 28) at Geneva University will be valuable in designing the AIDA connectors. Particular attention will be paid to the polishing and assembly stages, where quality assurance must be guaranteed and costs and schedule controlled.

The connector assembly for the AIDA TASD and MIND can be considered to be split in two main components:

1)   the connector which is embedded in the plastic scintillator and holds the fiber.
2)   the connector which houses the SiPM.

The first connector once glued onto the plastic scintillator bar provides a support enabling the polishing of the fiber ends. The second connector is designed to house the SiPM. In principle, the SiPM could be inserted into this second connector and held in place with a clip that applies pressure, ensuring contact between the SiPM bond pads and the connector pads, without having to solder the SiPMs. Given the number of SiPMs, it is worth designing a system that allows for recycling these to be used in another application if necessary.
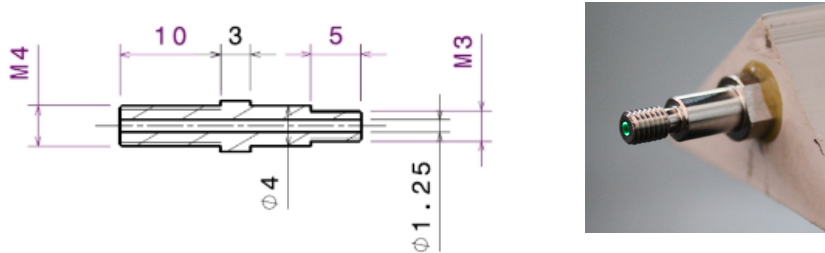
a)   b)

Figure 28:   The MICE EMR connector design is the basis for the design of the AIDA connector: a) dimensions of the EMR connector. b) photo of the EMR connector embedded in an EMR scintillator bar, shown with thread corresponding to M3 end of sketch a).
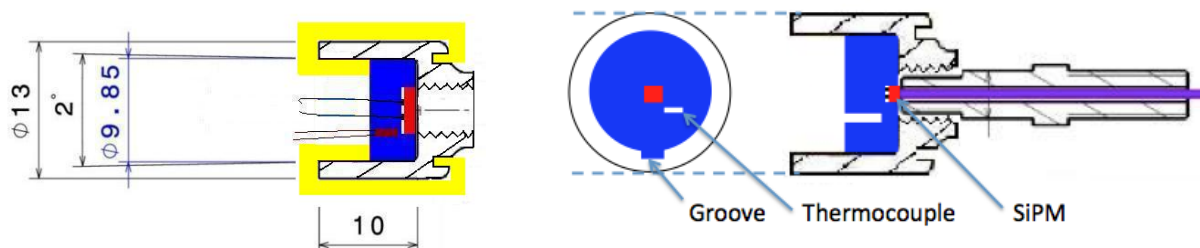
Figure 29:   Second connector which houses the SiPM, shown in red. The blue piece does not rotate with the external shell, but slides into a groove to hold the SiPM in place. The yellow piece also does not rotate and clips externally onto the outer shell to hold the blue piece + SiPM in place. A thermocouple can be optionally embedded in the blue piece.

What follows is an assembly sequence showing the main steps involved in the assembly of the plastic scintillator bars, fibers, connectors and SiPMs. The steps are illustrated in Figs. 30-32. Note that the **steps shown** are for a **double-ended** plastic scintillator bar! In its **final** implementation, each bar will more likely be read out from just **one end**. The other end can be covered by a reflective cap as shown in Figure 33.
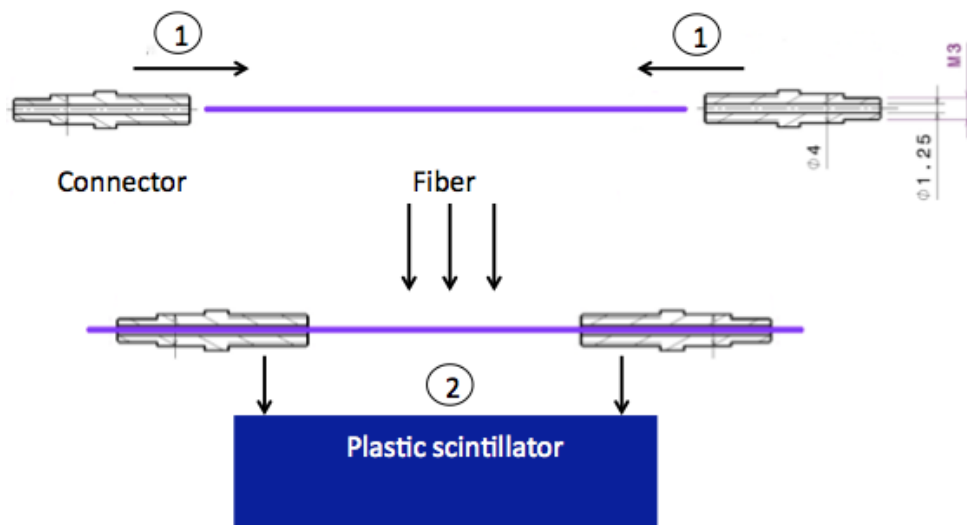
Figure 30:   Assembly sequences:

- ➢ *Step 1: Fitting fiber to connector.*
- ➢ *Step 2: Fitting connector and fiber to plastic scintillator.*

Figure 31:   Assembly sequences:

- ➢ *Step 3: Polishing fiber ends.*
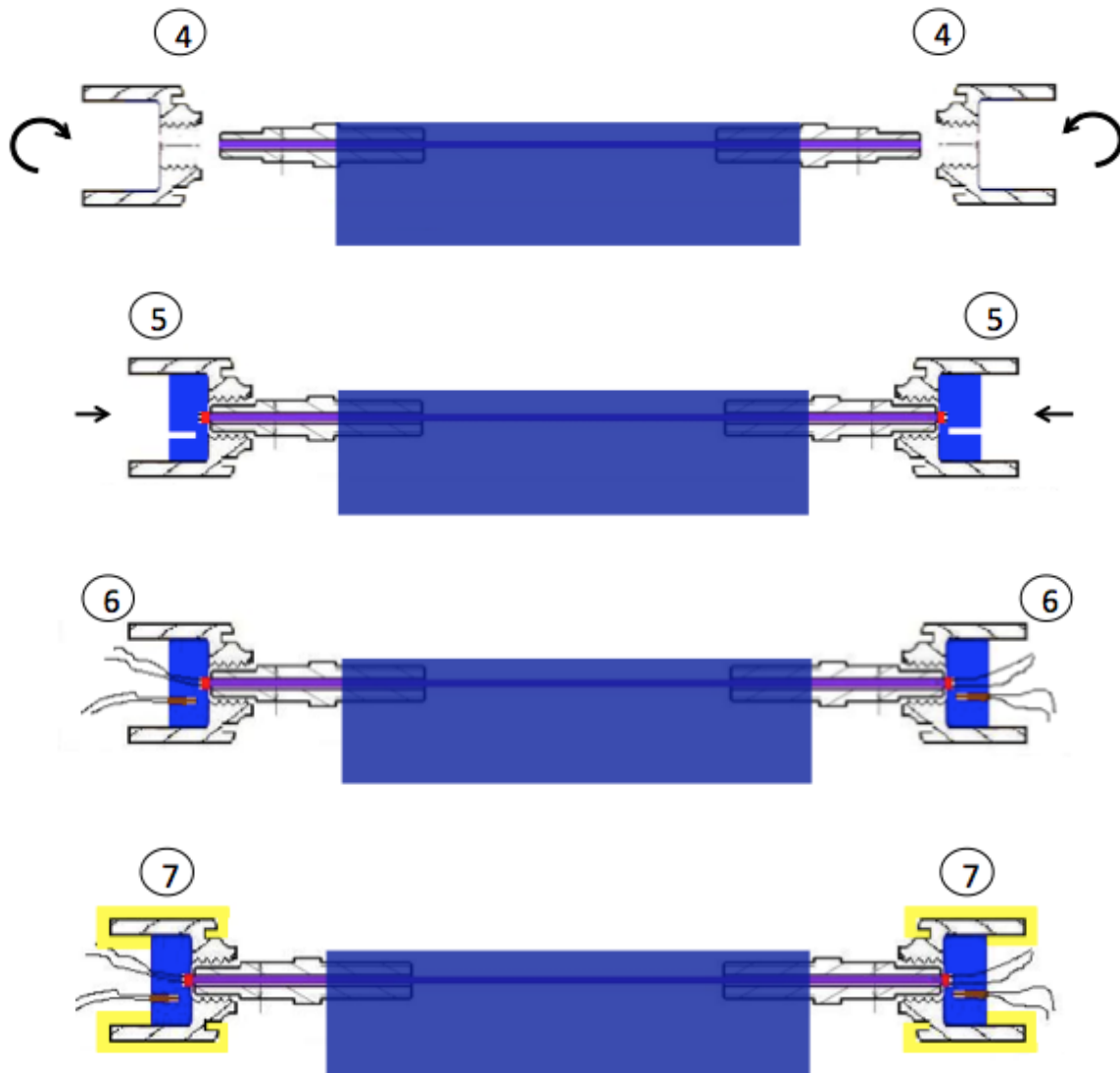
Figure 32:   Assembly sequences: Fitting the SiPM connectors:

> ➢ *Step 4: screwing on the SiPM connectors.*
> ➢ *Step 5: Fitting the SiPMs.*
> ➢ *Step 6: Fitting the thermocouples (optional).*
> ➢ *Step 7: Final clip to maintain SiPM in place.*

Figure 33:   Single-ended readout with SiPM of fiber embedded in a plastic scintillator bar.

7.3.   GENERAL METHODOLOGY FOR CHARACTERISING SIPM SIGNAL OUTPUT

A significant element of the characterisation of the plastic scintillator detector modules is a description of the processes that start with conversion of energy deposited to photons, and end with an output from the SiPMs and the subsequent shaping of that output. It is planned to write a simplified model as was done for PMTs by previous workers[11], drawing on experience gained by the T2K ND280 collaboration [12].

7.4.   LIGHT YIELD ESTIMATES

A series of simulations was carried out with FLUKA to estimate the energy deposited in a 1 cm-deep plastic scintillator, 3 cm wide. This information is widely available but nevertheless the simulations were carried out to cross-check the definition of simulation variables in preparation for more complex geometries. As expected, the energy deposited by a minimum ionising particle incident on a 1 cm-deep plastic scintillator slab is approx. 2 MeV, Figure 30.
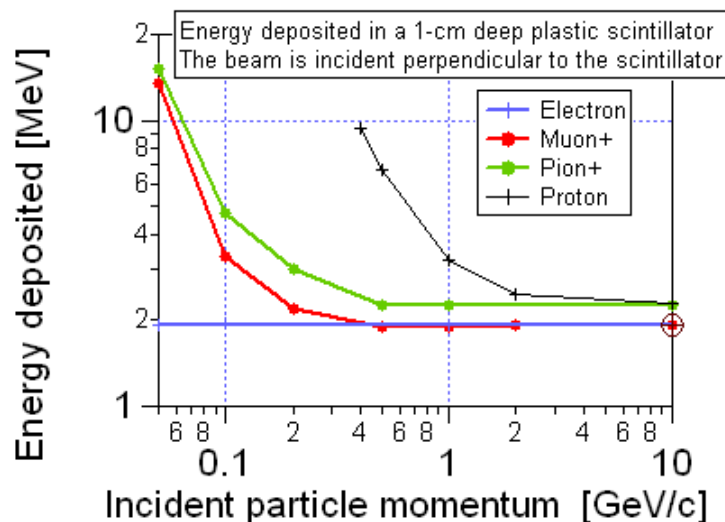
Figure 34:   Energy deposited in a 1-cm deep plastic scintillator. The particle beam was incident perpendicular to the surface of the plastic scintillator slab. The lateral volume of scintillator material was sufficient to contain showers.

Table 6: *Light yield estimates based on photon yield values from literature [11].*

Parameter	Unit	MICE EMR		AIDA	
		Perpendicular	Max.	Perpendicular	Max.
Scintillator bar parameters					
Shape	-	Triangular		Rectangular	
Bar length	[cm]	110		90	
Bar width	[cm]	3.3		1	
Bar height	[cm]	1.7		0.7	
Fibre length	[cm]	110	120	90	120
Energy deposition parameters					
Track length	[cm]	1.70	2.40	0.70	1.00
Peak Edep/cm	[MeV/cm]	8.82	8.82	8.82	8.82
Peak Edep	[MeV]	14.99	21.17	6.17	8.82
Edep/MIP/cm	[MeV/MIP/cm]	2.00	2.00	2.00	2.00
Edep/MIP	[MeV/MIP]	3.40	4.80	1.40	2.00
Photon conversion					
Photon yield	[ph/MeV]	1.25E+04	1.25E+04	1.25E+04	1.25E+04
Photon yield per bar	[ph]	1.87E+05	2.65E+05	7.72E+04	1.10E+05
Photon efficiency	%	5.00E-03	5.00E-03	5.00E-03	5.00E-03
Photons on SiPM	[ph]	9.37E+02	1.32E+03	3.86E+02	5.51E+02
MRS APD case					
PDE	%	35	35	35	35
Light yield	[p.e./MeV]	21.4	21.4	21.4	21.4
Total light yield	[p.e./bar]	320.8716	452.9952	132.1236	188.748
Specifications for minimum signal					
Min. p.e.	[p.e.]	1	1	1	1
Noise	[p.e.]	0.3	0.3	0.3	0.3

7.5. ELECTRONICS

Emphasis will be placed on the electronics options which offer the best opportunity for further development to cover medium-term foreseeable requirements for neutrino detectors and related applications.

The following are options for AIDA:

- DRS4: best long-term perspectives, requires some work to bring costs down.
- EASIROC: 3 kHz readout rate demonstrated, architecture close to EMR, cheap.
- T2K ND280 TRIP-t option: initially considered as the baseline but likely not retained for AIDA.

8. DATA ACQUISITION

The data acquisition system will be adapted from the MICE EMR DAQ [13].

9. PLANNING

9.1. COORDINATION

9.1.1. Task coordination

		Comment	Start	End
	Task review 1: Q4 2012		12/10/2012	12/14/2012
	Task review 2: Q1 2013		3/11/2013	3/15/2013
	Task review 3: Q2 2013		6/10/2013	6/14/2013
	Task review 4: Q3 2013		9/9/2013	9/13/2013
	Task review 5: Q4 2013		12/9/2013	12/13/2013
	Task review 6: Q1 2014		3/10/2014	3/14/2014
	Task review 7: Q2 2014		6/9/2014	6/13/2014
	Task review 8: Q3 2014		9/8/2014	9/12/2014
	Task review 9: Q4 2014		12/8/2014	12/12/2014

9.1.2. Proposal for TASD and MIND prototype detectors

		Comment	Start	End
	Proposal draft		9/3/2012	9/14/2012
	First review		9/14/2012	10/31/2012
	Final draft		11/1/2012	11/30/2012

9.1.3. Costing

		Comment	Start	End
	Costing review 1		9/24/2012	9/28/2012
	Costing review 2		6/24/2013	6/28/2013
	Costing review 3		6/23/2014	6/27/2014
	Costing review 4		1/12/2015	1/16/2015

9.1.4. SPS request for beam time

		Comment	Start	End
	Draft: SPS request		9/10/2012	9/14/2012
	Review: SPS request		9/17/2012	9/28/2012
	Submission: SPS request		10/1/2012	10/1/2012

9.1.5. Beam interface at H8

		Comment	Start	End
	Interface review		11/12/2012	11/16/2012
	Interface parameters		12/17/2012	12/21/2012

9.2. TASD DETECTOR PERFORMANCE

9.2.1. TASD simulations

		Comment	Start	End
	SiPM response simulations		1/1/2013	12/20/2013
	Software framework		9/3/2012	12/21/2012
	Flux driver		9/3/2012	1/30/2015
	Event generator		9/3/2012	1/30/2015
	Transport		9/3/2012	1/30/2015
	Digitisation		9/3/2012	1/30/2015
	Energy reconstruction		9/3/2012	1/30/2015
	Track reconstruction		9/3/2012	1/30/2015

9.2.2. TASD offline runs

		Comment	Start	End
	Sub-detector cosmic run		2/17/2014	10/1/2014
	Full detector cosmic run		9/15/2014	10/1/2014

9.2.3. TASD online operation

		Comment	Start	End
	TASD online tests		10/13/2014	11/3/2014
	TASD online runs		12/1/2014	12/31/2014

9.3. MIND DETECTOR PERFORMANCE

9.3.1. MIND simulations

		Comment	Start	End
	SiPM response simulations		1/1/2013	12/20/2013
	Software framework		9/3/2012	12/21/2012
	Flux driver		9/3/2012	1/30/2015
	Event generator		9/3/2012	1/30/2015
	Transport		9/3/2012	1/30/2015
	Digitisation		9/3/2012	1/30/2015
	Energy reconstruction		9/3/2012	1/30/2015
	Track reconstruction		9/3/2012	1/30/2015

9.3.2. MIND magnetisation

		Comment	Start	End
	MIND B-field 2D simulations		9/3/2012	10/31/2012
	MIND B-field 3D simulations		10/1/2012	6/28/2013
	MIND B-field measurements		5/19/2014	5/30/2014

9.3.3. MIND offline runs

		Comment	Start	End
	MIND sub-detector cosmic run		3/10/2014	8/29/2014
	MIND full detector cosmic run		8/18/2014	8/29/2014

9.3.4. MIND online operation

		Comment	Start	End
	MIND online tests		1/1/2015	1/11/2015
	MIND online runs		1/12/2015	1/30/2015

9.4. ELECTRONICS AND DAQ

9.4.1. SiPM

		Comment	Start	End
	SiPM comparison/characterisation		10/8/2012	12/21/2012
	SiPM procurement		1/7/2013	6/28/2013
	SiPM QA		7/1/2013	12/20/2013

9.4.2. Electronics architecture

		Comment	Start	End
	Architecture definition		9/3/2012	9/28/2012
	Electronics interfaces		1/7/2013	3/29/2013

9.4.3. Readout chip

		Comment	Start	End
	RoC R&D proposal		9/3/2012	9/28/2012
	RoC R&D		10/1/2012	3/28/2014

9.4.4. Front-end board

		Comment	Start	End
	FEB design		9/2/2013	10/31/2013
	FEB production and QA		10/1/2013	2/28/2014
	FEB VHDL programming		9/2/2013	2/28/2014

9.4.5. Back-end board

		Comment	Start	End
	BEB design		4/1/2013	4/30/2013
	BEB production and QA		10/1/2013	3/31/2014
	BEB VHDL programming		9/2/2013	2/28/2014

9.4.6. DAQ

		Comment	Start	End
	DAQ concept		12/17/2012	12/21/2012
	DAQ implementation		1/6/2014	3/31/2014

9.5. COMMON HARDWARE

9.5.1. Scintillators

		Comment	Start	End
	Scintillator prototyping		10/1/2012	12/21/2012
	Scintillator manufacturing		1/7/2013	7/31/2013

9.5.2. Fibers

		Comment	Start	End
	Fiber choice		10/1/2012	10/31/2012
	Fiber procurement		1/1/2013	7/31/2013

9.5.3. Connectors

		Comment	Start	End
	Connector design		9/3/2012	12/21/2012
	Connector manufacturing		4/1/2013	6/28/2013

9.5.4. Scintillator bar assembly

		Comment	Start	End
	Fiber cutting		7/1/2013	1/31/2014
	Fiber gluing		7/1/2013	1/31/2014
	Fiber polishing		9/16/2013	2/28/2014
	Assembly SiPM+connector+scintillator+fiber		10/1/2013	1/31/2014
	Scintillator bar test (assembled)		10/1/2013	2/28/2014

9.5.5. Scintillator module support structure

		Comment	Start	End
	Sci module mechanical design		1/1/2013	3/29/2013
	Sci module mechanical support procurement		9/23/2013	10/18/2013
	Sci module assembly		2/3/2014	5/2/2014

9.6. TASD HARDWARE

9.6.1. Accordion mechanics

		Comment	Start	End
	Accordion mechanics design		1/1/2013	3/29/2013
	Accordion mechanics construction		9/2/2013	12/31/2013

9.6.2. Morpurgo magnet integration

		Comment	Start	End
	Morpurgo integration dummy test		1/6/2014	1/9/2015
	Morpurgo integration final		9/1/2014	9/5/2014
	Morpurgo module dismantling		1/5/2015	1/9/2015

9.7. MIND HARDWARE

9.7.1. Iron plate procurement

		Comment	Start	End
	Dimensioning		9/3/2012	9/21/2012
	Iron shortlist		9/3/2012	9/21/2012
	Iron final order		9/24/2012	9/28/2012
	Temporary storage		10/1/2012	12/31/2013

9.7.2. Conductor coil procurement

		Comment	Start	End
	Coil study		4/1/2013	4/26/2013
	Coil tendering/ordering		5/6/2013	5/31/2013

9.7.3. Iron plate design

		Comment	Start	End
	Design of B-field probe inserts		1/7/2013	2/28/2013
	Coupling to support structure		9/2/2013	12/20/2013

9.7.4. MIND craddle structure

		Comment	Start	End
	MIND craddle design		9/2/2013	12/20/2013
	MIND craddle construction		1/6/2014	1/31/2014

9.7.5. Power supply

		Comment	Start	End
	Power supply specification		4/1/2013	4/26/2013
	Power supply obtention		4/1/2014	1/30/2015

9.7.6. MIND assembly

		Comment	Start	End
	MIND assembly: steel + coils		3/3/2014	3/21/2014
	MIND assembly: sci modules		1/5/2015	1/9/2015

10. COSTING

Shown in Table 7 are equipment costs for the TASD and MIND prototype detectors. As can be seen, a large fraction of the total costs lie in the detector modules and associated electronics. In order not to duplicate these costs, it was decided to use the same detector modules in both the TASD and the MIND and therefore operate the two prototypes separately.

Table 7:   Costing of the TASD and MIND prototype detectors. Only equipment costs are included in the breakdown of costs presented here.

Item	Quantity	Cost [CHF]	Quote [Yr]
Common items to both TASD and MIND			
Plastic scintillators	10000	40'000.-	-
SiPM	10000	90'936.-	2012
WLS fiber	10000 m	62'768.-	2012
SiPM connectors	20000	35'000.-	2012
Detector module mechanics	50	20'000.-	2012
Electronics & DAQ	10000	200'000.-	-
TASD specific items			
TASD mechanics	-	40'000.-	2012
MIND specific items			
Iron	-	76'532.-	2012
Engineering of iron plates	-	100'000.-	2012
Magnet coils	-	10'000.-	-
Power supply	-	0.-	-

11. ACKNOWLEDGEMENTS

Several people have contributed to the work presented in this document, notably Prof. Yury Kudenko and co-workers at the INR, Ryan Bayes of Glasgow university on the MIND simulations and Rosen Matev of Sofia university on the TASD simulations. I would particularly like to thank Jeremy Bauche and Maxime Dumas of the CERN-TE-MSC-MNC section for their work on the magnetisation of the MIND. All those involved at Geneva university are gratefully acknowledged.

12. REFERENCES

[1]   F.P. An et al., Observation of electron-antineutrino disappearance at Daya Bay, arXiv:1203.1669.

[2]   S-B. Kim, Observation of Reactor Electron Antineutrino Disappearance in the RENO experiment, arXiv:1204.0626.

[3]   Expression of Interest for a very long baseline neutrino oscillation experiment (LBNO), CERN-SPSC-2012-021, SPCS-EOI-007.

[4]   ICARUS and NESSIE collaborations, Search for "anomalies" from neutrino and anti-neutrino oscillations at $\Delta m^2 \approx 1 eV^2$ with muon spectrometers and large LAr-TPC imaging detectors. Technical Proposal, CERN –SPSC-2012-010 and SPSC-P-347, March 2012.

[5]   Long-Baseline Neutrino Experiment (LBNE) Project, Conceptual Design Report, October 2012.

[6]   The Hyper-Kamiokande Experiment Detector Design and Physics Potential, Letter of Intent, arXiv:1109.3263, 15 September 2011.

[7]   Neutrinos from STORed Muons, Letter of Intent, arXiv:1206.0294, June 2012.

[8]   International Design Study for a Neutrino Factory, Interim Design Report, IDS-NF-020, 19 March 2011.

[9]   A. Cabrera, Systematic Comparison of the MINOS Near and Far Detector Readout Systems, PhD Thesis, 2005.

[10]   AIDA Milestone Report MS27, March 2012.

[11]   F. Sanchez & G. Medina-Tanco, Modeling scintillator and WLS fiber signals for fast Monte Carlo simulations, NIM A 620 (2010) 182-191.

[12]   A. Vacheret et al., Characterization and simulation of the response of Multi-Pixel Photon Counters to low light levels, NIM A 656 (2011) 69-83.

[13]   EMR Readout scheme v2.0, April 2011.